Unravelling the complexity of magma plumbing at Mount St Helens: a new trace element partitioning scheme for amphibole

Madeleine. C. S. Humphreys[1*], George. F. Cooper[1], Jing Zhang[1,2], Matthew Loewen[3,4], Adam. J. R. Kent[3], Colin. G. Macpherson[1] and Jon. P. Davidson[1§]

[1]Department of Earth Sciences, University of Durham, Durham, DH1 3LE, UK

[2]State Key Laboratory of Lithospheric Evolution, Institute of Geology and Geophysics, Chinese Academy of Sciences, Beijing, 100029, China

[3]College of Earth, Ocean and Atmospheric Sciences, Oregon State University, Corvallis, OR 97330, USA

[4] Alaska Volcano Observatory, U.S. Geological Survey, Anchorage, AK 99508, USA

*Corresponding author. E-mail: madeleine.humphreys@durham.ac.uk

§ Deceased

ABSTRACT

Volcanoes at subduction zones reside above complex magma plumbing systems, where individual magmatic components may originate and interact at a range of pressures. Because whole rock compositions of subduction zone magmas are the integrated result of processes operating throughout the entire plumbing system, processes such as mixing, homogenisation and magma assembly during shallow storage can overprint the chemical signatures of deeper crustal processes. Whereas melt inclusions provide an effective way to study the uppermost 10-15 km of the plumbing system, challenges remain in understanding magma intrusion, fractionation and hybridisation processes in the middle to lower crust (15-30 km depth), which commonly involves amphibole crystallisation. Here, we present new insights into the mid-crustal plumbing system at Mount St Helens, USA, using multiple regression methods to calculate trace element partition coefficients for amphibole

phenocrysts, and thus infer the trace element compositions of their equilibrium melts. The results indicate vertically distributed crystal fractionation, dominated by amphibole at higher pressures and in intermediate melts, and by plagioclase at lower pressures. Variations in Nb, Zr and REE concentrations at intermediate SiO_2 contents suggest repeated scavenging of partially remelted intrusive material in the mid-crust, and mixing with material from geochemically diverse sources. Amphibole is an effective probe for deep crustal magmatism worldwide, and this approach offers a new tool to explore the structure and chemistry of arc magmas, including those forming plutonic or cumulate materials that offer no other constraints on melt composition.

KEYWORDS

Trace elements; partitioning; amphibole; subduction zones; Mount St Helens; magma plumbing

INTRODUCTION

Subduction zone volcanoes produce some of the most petrographically and geochemically complex igneous rocks of any tectonic setting. This complexity arises from the diversity of processes operating from melt generation, through crustal storage and differentiation, to magma transport and eruption. An accurate understanding of these subterranean magmatic processes is essential for interpreting the eruptive behaviour and hazards of volcanoes, as well as the formation and evolution of the continental crust. Knowledge of the complexities of a volcanic plumbing region can also aid interpretation of geophysical observations, as well as any temporal changes in eruptive products. Geophysical studies commonly indicate the presence of low-seismic velocity or low resistivity regions in the middle to deeper crust, that may be linked to the presence of fluids or melt (e.g. Pritchard and Gregg 2016). Both geophysical and experimental studies also suggest that the lower crust at arcs may be dominated by mafic minerals, including amphibole (Holbrook et al. 1992; Melekhova et al. 2015; Müntener and Ulmer 2018), and this is corroborated by studies of exposed arc sections (e.g. DeBari and Greene 2011). However, this information can be hard to integrate with petrology, which tends to yield information mainly about processes in the uppermost 10-15 km of the crust. We need, therefore, to

develop new petrological methods to interrogate processes operating within the deeper regions of the crust at subduction zones.

Mount St Helens volcano, Washington, USA, is one of the most extensively studied and well monitored subduction zone volcanoes in the world. It has been active for at least 272,000 years based on K-Ar and Ar-Ar ages (Clynne et al. 2008; Clynne personal communication) but zircon ages >500 ka (Claiborne et al. 2010) suggest that the magmatic system in general has been active for significantly longer. The explosive eruption of 1980 resulted in significant disruption to the regional economy and infrastructure, as well as fatalities (Mason et al. 1980), and was followed by an extended period of unrest and dome growth. The structure and form of the plumbing system underneath the volcano is still debated. Several geophysical studies linked to the recent iMUSH project (Witze 2014) have recognised broad regions of the deep crust (15-35 km) with seismic velocity anomalies that have been interpreted as indicating the presence of melt (Hill et al. 2009; Kiser et al. 2016; Flinders and Shen 2017), together with deep long-period earthquakes suggesting movement of magma and/or magmatic fluids (Nichols et al. 2011). Petrological studies have shown that the 1980-2006 dacites from Mount St Helens represent hybrid magmas with multiple crystal populations from diverse sources (e.g. Berlo et al. 2007; Streck et al. 2008; Thornber et al. 2008; Wanke et al. in press), inherited from different crustal sources and melting processes. This diversity of petrologic products hints at a role for deep crustal processes, as seen in the geophysical imaging. In contrast, melt inclusions show that the magmas were erupted from storage regions in the upper crust, with recorded volatile saturation pressures of 120 to 240 MPa (Blundy and Cashman 2001, 2005; Blundy et al. 2008) (5-10 km). This disconnect between geophysical and petrological investigations implies a gap in our knowledge about the locations of melt differentiation, magma storage, and final assembly and homogenisation.

Here, we present new details on processes operating throughout the arc crust beneath Mount St Helens, using an innovative partitioning scheme that inverts the trace element chemistry of amphiboles to yield equilibrium melt compositions. Amphibole is one of the most important mafic

minerals to form in the mid- and deep crust at arcs: it occurs early in the fractionation sequence of many arc magmas and crystallises at moderate to high pressures (Nandedkar et al. 2016). Our approach is to build multiple-regression relationships from a database of existing experimental amphiboles, to link the partition coefficients of commonly used trace elements to the major element chemistry of the amphibole. This method enables us to develop new insights into processes operating in less evolved (andesitic) melts at relatively high pressures (mid- to lower crust). We show that the magmatic system under Mount St Helens is dominated by mafic minerals including amphibole (± clinopyroxene ± Fe-Ti oxides) in the mid-crust, and by plagioclase (± Mg-hornblende) at low pressures (<300 MPa). The compositions of amphibole equilibrium melts allow us to identify the signatures of mid-crustal assimilation of older intrusive magmatism, which are blended together during final magma assembly. This approach enables us to build a picture of the vertical extent and progressive geochemical homogenisation of diverse magmatic components within the deeper volcanic plumbing system.

METHODS

Amphibole structure and chemistry

Amphibole is a common constituent of arc magmas and is particularly common in mafic to intermediate magmas crystallising at high pH_2O. This means it has the potential to record the evolving chemical compositions of subduction zone magmas. The chemical composition of any magmatic mineral depends on intrinsic parameters such as pressure, temperature and fO_2, as well as the major- and trace-element composition of its host melt. However, using this information to interpret magmatic processes relies on a quantitative understanding of the partitioning behaviour of trace elements between mineral and coexisting melt.

The double-chain crystal structure of amphibole can be described as:

$$A\ B_2\ C_5\ T_8\ O_{22}\ (OH, F, Cl)_2$$

and includes several crystallographic sites with different coordination and size (Leake et al. 1997), that can accommodate a range of trace elements, including large ion lithophile elements (Rb, Sr, Ba),

Pb, U, Th, high field strength elements (Ti, Zr, Hf, Nb and Ta), rare earth elements (REE) and Y, and transition metals (e.g. (Tiepolo et al. 2007). In terms of major element chemistry, Si and Al are the dominant components of the tetrahedral (T) site; Mg, Fe (both Fe^{2+} and Fe^{3+}), Ti, Mn and Al occupy the small-medium octahedral (M1-3, 'C') sites; the larger octahedral (M4, 'B') site is dominated by Ca and Na; and Na also sits in the partially filled 'A' site together with K. For the trace elements, Rb, Ba and Pb have high ionic radius and are accommodated in the A site, while Sr can occur at either A or M4 (Tiepolo et al. 2007). Tetravalent HFSE (Zr^{4+} and Hf^{4+}) are incorporated onto M2 by substitution for Ti (Oberti *et al.*, 2000) while Nb and Ta are incorporated preferentially into M1 (Tiepolo *et al.*, 2000b). REE and Y are thought to be partitioned into M4, substituting for either Ca and/or Na (Brenan et al. 1995; Klein et al. 1997; Hilyard et al. 2000; Shimizu et al. 2017).

This strong crystal-chemical control on trace element partitioning means that variations in raw amphibole trace element abundances can result either from real variations in the coexisting melt composition during crystallisation, *and/or* from variations in amphibole major element chemistry at fixed melt composition. Previous work shows that trace element partitioning in amphibole is related to the degree of melt polymerization (Tiepolo et al. 2007; Nandedkar et al. 2016) but, in general, the complexity of the amphibole crystallographic structure means that these controls are poorly understood. Furthermore, for petrological studies a primary aim is typically to retrieve *unknown* melt compositions from analyses of naturally occurring crystals; therefore the degree of melt polymerization is generally not known. Instead we focus on the crystal-chemical controls on partitioning outlined above, and use multiple regression (MR) methods on a large experimental dataset drawn from the literature (table 1; Figure 1) to calculate trace element partition coefficients for amphibole from the major element composition of the crystal. This enables us to predict the trace element composition of its equilibrium host melt ("amphibole equilibrium melts", AEM). We used a version of our earlier multiple regression study (see supplementary information; Zhang et al. 2017) to find the corresponding major element chemistry of the AEM.

Multiple regression analysis

For the MR analysis, we used $^{Amph/L}D$ values reported in 13 experimental studies conducted over a wide range of conditions (200-2,500 MPa, 780-1,100 °C, figure 1, table 1), using starting compositions from basanite to rhyolite (Table 1; Figure 1). The experiments crystallised calcic amphiboles in the range Pargasite – Edenite – Hastingsite - Magnesiohastingsite (MgHst) – Kaersutite – Tschermakite (Tsch) – Magnesiohornblende (MgHbl). Obvious outliers were removed prior to regression.

We carried out the MR analysis using the statistical software package R (R Core Team 2013), and specifically the package '`robustbase`' which includes routines to minimise the effects of outliers during regression. Here we focus on temperature-independent regressions because temperature is rarely known independently (or precisely) for petrological studies. Temperature undoubtedly can affect partitioning (e.g. Green and Pearson 1985; Klein et al. 1997); therefore, we include temperature-dependent regressions, for those elements where temperature was a statistically significant parameter in the results (see supplementary information). We do not consider these further but they are presented for completeness.

In the regression analysis, the natural logarithms of $^{Amph/L}D$ (lnD) were treated as dependent variables. Amphibole stoichiometric formula components were considered as independent variables, including tetrahedral Si (Si_T); M1-3 site Al (Al_{VI}), Ti, Fe^{3+}, and Fe^{2+}; M4 site Ca (Ca_{M4}) and A-site Na (Na_A). Tetrahedral-site Al (Al_T), Mg and Na_{M4} were excluded to avoid the issue of strong multi-colinearity (following Zhang et al. 2017). Although some multi-colinearity between variables remains (most commonly between Fe^{3+} and Fe^{2+}), this does not preclude successful application of the results, though it does limit physical interpretation of trace element site occupancy (not a primary aim of our study). We did not consider Cr and Mn (hosted in M1-3) or K (hosted in A site), due to their minor abundances in amphibole and thus high relative analytical uncertainties. Because amphibole stoichiometric formula calculations depend on ferric iron content, and the experiments cover a wide range of fO_2 (e.g. from haematite-magnetite to magnetite-wüstite buffer, (Green and Pearson 1985) we used the 'average Fe^{3+}' approach (Leake et al. 1997) to calculate ferric and ferrous components,

following (Zhang et al. 2017). While this approach remains relatively inaccurate, it is better than assuming Fe_T = FeO (Schumacher 1991; Hawthorne and Oberti 2007; Locock 2014). Direct measurement of $Fe^{3+}/\Sigma Fe$ in amphibole remains difficult, requiring Mössbauer or synchrotron methods such as XANES (e.g. Dyar et al. 2016) and such measurements are rarely available. We emphasise that replacing Fe^{3+} and Fe^{2+} with total Fe (Fe_T) in the regression does not significantly affect the accuracy or precision of the regressions. All MR equations presented have residual standard error (RSE) between 0.19-0.49 (Table 2). As a check of accuracy, the predicted partition coefficients were plotted against the measured experimental partition coefficients, together with calculated 1σ and 2σ prediction intervals, and show good agreement (Figure 2; table 2; supplementary figures 1 and 2).

Multiple regression equations

Statistically significant MR results were retrieved for LILE (Rb and Sr), Pb, HFSE (Zr and Nb), REE (La, Ce, Nd, Sm, Gd, Dy, Ho, Er, Yb, Lu) and Y. The output of each MR analysis is given as the intercept and coefficients of the nominated independent variables, from which a multiple regression equation can be derived (Table 2). For example, the equation for the prediction of ${}^{Amph/L}D_{Nb}$ (Eq. 5) is expressed as:

$$ {}^{Amph/L}D_{Nb} = \exp(-22.27 + 2.3241Si + 2.9786\ Fe^{3+} + 1.44\ Fe^{2+} + 3.7633\ Ti + 1.8719\ Ca) $$

This equation enables the Nb content of the amphibole equilibrium melt to be calculated, based on knowledge of the amphibole major element composition (because this affects the structure and trace element capacity of different crystallographic sites). The values of D_{REE} calculated using our MR approach are similar to those derived by Shimizu et al. (2017) using a lattice strain model. Statistically significant regressions could not be retrieved for several elements including Ba, Cs, Hf, Ta, and Sc, typically because of low concentrations and a paucity of calibration data. A template for calculation of partition coefficients using these methods is provided in the supplementary information.

Electron microprobe analyses

Amphiboles from the 1980-1986 eruption of Mount St Helens were analysed in polished 25 mm epoxy rounds or standard polished thin sections. Major element analysis was carried out using a Cameca SX-100 electron microprobe at Oregon State University. All analyses used a 1 μm beam diameter, 30 nA beam current and 15 kV accelerating voltage. Count times were 60 seconds for Cl, 30 seconds for Mg, Ca, Ti, Mn, Fe, Al, and S, 20 seconds for F, K, and P, and 10 seconds for Na and Si. Sodium, Si, and K were corrected to zero time intercepts. Background count times were half the peak times. Kakanui hornblende (USNM 143965) was used as a secondary standard to check the accuracy of the calibration.

Laser ablation inductively coupled plasma mass spectrometry

Trace element analysis of amphiboles was done by LA-ICP-MS at Oregon State University using an ArF 193 nm Photon Machines G2 laser ablation system and a Thermo Scientific X-Series2 quadrupole ICP-MS following Loewen and Kent (2012). Amphiboles were analyzed using a 30 or 50 μm spot pulsed at 7 Hz for approximately 30 seconds. Standard reference material GSE-1G was used as a calibration standard and GSD-1G, BHVO-2G, and BCR-2G were monitored as secondary standards. Ca (from EPMA analyses) was used as the internal standard.

RESULTS

Trace elements in Mount St Helens amphiboles and predicted melts

We collected new major- and trace element analyses of amphiboles from Mount St. Helens dacites erupted during May – August 1980 (including samples from Cashman and McConnell 2005), and also processed published amphibole data from the 2004-2006 eruption (from Thornber et al. 2008). Most amphiboles are MgHst-Tsch with a smaller population of MgHbl. MgHbl have Mg-numbers from 0.62 to 0.76 ($Mg/Mg+Fe^{2+}$) and $(Na+K)_A$ of 0.32 to 0.58, whereas MgHst-Tsch have Mg-numbers from 0.65 to 0.84 and (Na+K)A of 0.39 to 0.61 (supplementary table). Trace element contents of the amphiboles range from ~70-300 ppm Sr, 12-100 ppm Ba, ~20-150 ppm Zr, 1-30 ppm Nb and 15-80

ppm Y (supplementary table 2). Amphibole REE contents for the 1980 eruptions were analysed in the same laboratory as those reported by (Thornber et al. 2008) and (Rowe et al. 2008), and their compositions are consistent, typically in the range 1-10 ppm La and 2-15 ppm Sm.

The major element compositions of AEM were calculated following the approach of our previous MR analysis results (see supplementary dataset for regression equations used; Zhang et al. 2017). Compositions of AEM range from ~60 to 75 wt% SiO_2, and overlap with previously published andesitic to dacitic whole rocks and with the less evolved (rhyodacite) end of the melt inclusion field (Figure 3). SiO_2 contents are similar to those inferred using the approach of Ridolfi and Renzulli (2012). MgHbl yield the most evolved AEM, with relatively high SiO_2, and these agree well with the compositions of plagioclase-hosted melt inclusions (Blundy et al. 2008; 69-76 wt% SiO_2, 1.6-2.7 wt% FeO, 2.3-3.2 wt% K_2O, 1.8-2.9 wt% CaO and 0.3- 0.65 wt% MgO, Figure 3). AEM for Tsch-MgHst are more primitive (58-69 wt% SiO_2) and extend the melt inclusion trends backwards to overlap with Mount St Helens whole rocks (Figure 3).

Trace element partition coefficients were calculated from equations constructed using the parameters presented in table 2. These partition coefficients were then used to calculate the trace element compositions of amphibole equilibrium melts. The calculated partition coefficients for Mount St Helens amphiboles varied from 0.29 to 0.49 for Sr, from 0.14 to 1.0 for La, from 1.3 to 4.37 for Y and from 0.3 to 2.4 for Nb (supplementary information). This variation is a result of the variable major element chemistry of the crystals (or of zones within individual crystals) and emphasises the importance of correcting for the effects of major element chemistry on trace element partitioning (Figure 4). The majority of trace element analyses yield AEM compositions (supplementary table) that fit very well with both melt inclusions and whole rocks (see Blundy et al. 2008 for melt inclusions, and Blundy et al. 2008, Wanke et al. in press and Wanke et al. 2019 for sources of compiled whole rock data for Mount St Helens). There are two exceptions. First, despite having a statistically significant regression, calculated partition coefficients for Rb give very low predicted melt concentrations (typically 2-10 ppm) that do not agree with melt inclusion compositions (~40-50

ppm); the reason for this is not clear. Second, a subset of analyses gives AEMs with trace element concentrations up to 2-3 times higher than the main population (Figure 5), typically at intermediate silica (59-68 wt% SiO_2); this will be discussed further below.

Dealing first with the main body of AEM compositions, Sr contents decrease continuously with increasing SiO_2, projecting from the whole-rocks towards the plagioclase-hosted melt inclusions (Figure 5), and suggesting compatible behaviour. The melt inclusions also show decreasing Sr contents with increasing SiO_2, but with a steeper gradient than the AEMs (Figure 5). This is important because it likely indicates a change in the crystallising assemblage (see below). The other trace elements show variably incompatible behaviour. The rare earth element concentrations of AEM overlap well with the more evolved whole rocks and the less evolved melt inclusions but are scattered and typically show no significant variations with SiO_2, whereas the melt inclusions increase strongly (Figure 5). In the 2004-2006 dataset (Thornber et al. 2008) MgHst-Tsch yield AEM similar to the 1980 eruptions, whereas MgHbl yield AEM with a similar range of LREE but slightly lower average MREE and HREE concentrations (Figure 5). Similarly, Nb and Zr show little change with increasing SiO_2 (perhaps increasing slightly) and correlate well with each other. Zircon concentrations in the AEM are typically lower than those in the whole rocks (Figure 5), though there is some overlap as well as considerable scatter. In contrast, the Nb and Zr concentrations of melt inclusions increase more strongly with increasing differentiation (Figure 5).

Superimposed on these general patterns is considerable variability towards higher incompatible element concentrations, mainly at intermediate silica (59-68 wt% SiO_2), as mentioned above. This is most striking for Nb (up to 30 ppm), La (up to 37 ppm) and Zr (up to 306 ppm) but is also observed for other REE and Y (Figure 5). These significantly higher melt trace element concentrations are nonetheless similar to those of rare melt inclusions (Blundy et al. 2008) and some whole rocks (Leeman et al. 1990; Wanke et al. in press; Wanke et al. 2019). We were not able to produce statistically reliable AEM regressions for Ba, but the Ba concentrations of amphiboles correlate

strongly with Nb and Zr in the amphiboles. We would therefore also expect that Nb-rich AEM may also have anomalous Ba contents.

Both Sm/Yb and La/Yb of AEM are essentially constant with increasing SiO_2, and again agree well with both whole-rock and melt inclusions, in particular for La/Yb (Figure 6). In both cases, some anomalous values are seen, in particular to high La/Yb at intermediate SiO_2. As with the HFSE, these anomalous values are consistent with rare melt inclusion compositions (Figure 6).

DISCUSSION

Upper crustal fractionation of dacites

Amphibole equilibrium melts calculated from MgHbl are rhyodacitic, equivalent to the major element compositions of less evolved melt inclusions, while MgHst-Tsch amphiboles are calculated to be in equilibrium with andesite to dacite melts. The Sr concentrations of AEM from MgHbl coincide with the Sr contents of melts in equilibrium with plagioclase phenocryst rims from the 1980s magmas (150-300 ppm, Berlo et al. 2007), and with melt inclusion Sr concentrations. The Sr concentrations of AEM decrease with increasing SiO_2, and AEM from MgHbl also have low Eu/Eu* (Figure 7), indicating a strong negative Eu anomaly. Taken together, this is good evidence that the latest stages of fractionation (phenocryst growth, but prior to crystallisation of the dacite groundmass) involve rhyodacite melt crystallising abundant plagioclase and minor MgHbl at low to moderate pressures, which would stabilise plagioclase (e.g. Rutherford et al. 1985; Moore and Carmichael 1998; Martel et al. 1999; Blundy and Cashman 2001; Prouteau and Scaillet 2003). Fractionation dominated by plagioclase ± hornblende is also consistent with the low bulk partition coefficients for Zr, Nb and Yb that are required to generate significant enrichment during progressive crystallisation, as observed in the melt inclusions. This general picture is consistent with existing understanding of the genesis of the dacites (e.g. Pallister et al. 2008; Blundy et al. 2008) and therefore gives confidence that the amphibole equilibrium melts are able to retrieve useful information about the magmatic system. We

note that the fractionation of minor orthopyroxene in the dacites probably has little effect on REE and HFS concentrations, and our AEM calculations are therefore relatively insensitive to this.

Generation of intermediate magmas

The variation of Eu/Eu* in the AEM from MgHst-Tsch (Figure 7) indicates that plagioclase was also crystallising actively at intermediate SiO_2, but the rate of Sr decrease with increasing SiO_2 is lower than it is for the melt inclusions, suggesting that a lower proportion of plagioclase was fractionating during crystallisation of the MgHst-Tsch than for the MgHbl. However, the whole rocks lack a Eu anomaly (Figure 7), and some have higher Sr contents than MgHst-Tsch AEM, despite having similar SiO_2 contents (Figure 5). This supports suggestions that the bulk rocks contain some feldspar 'crystal cargo', in other words antecrystic material that is carried by the host melt (Blundy et al. 2008). The Sr contents of intermediate AEM are consistent with those in equilibrium with most plagioclase cores from the 1980s magmas (300-400 ppm), while the least evolved AEM have Sr concentrations similar to those of unusually calcic, boxy-cellular plagioclase cores (An_{67-82}, 400-530 ppm Sr, Berlo et al. 2007). Similar plagioclase textures have been observed elsewhere including at Karymsky, Kamchatka (Izbekov et al. 2002) and Colima, Mexico (Crummy et al. 2014) and have been variably attributed to resorption during decompression (e.g. Nelson and Montana 1992); to resorption during mixing with more primitive melts (Nakamura and Shimakita 1998; Izbekov et al. 2002); and to rapid skeletal growth (for a summary see Streck 2008). For Mount St Helens, we interpret the overlap of MgHst-Tsch AEM with plagioclase equilibrium melts (from Berlo et al. 2007) as an indication that these cellular textures formed through mixing with more primitive (andesitic) melts within the volcanic plumbing system, perhaps during mingling with more primitive hybrid basalts (Wanke et al. in press; Wanke et al. 2019; see also below). Therefore the magmas arrive in the shallow system already carrying a significant quantity of crystalline material, including both plagioclase crystals (which go on to grow new rims in the shallow storage region) and amphibole. This is also consistent with U-series ages for plagioclase which indicate mechanical mixing of older recycled crystals and younger overgrowths (Cooper and Reid 2003).

The most primitive whole-rocks erupted from Mount St Helens (<55 wt% SiO_2) are geochemically and isotopically heterogeneous, including an HFSE-enriched, intraplate-like component with elevated TiO_2 and P_2O_5 and high La/Yb (Leeman et al. 1990; Smith and Leeman 1993; Bacon et al. 1997; Leeman and Smith 2019; Wanke et al. 2019), as well as low-K olivine tholeiites with much lower La/Yb (Wanke et al. 2019) and arc-type basaltic andesites with moderate La/Yb and depletion in HFSE (Wanke et al. 2019). This diversity has been attributed to the result of decompression melting of a heterogeneous, variably enriched mantle source region (Leeman & Smith 2019) with water-poor margins producing HFSE-enriched magmas (Wanke et al. 2019). Domains that are either metasomatised (Leeman et al. 2005) or experience greater contributions from slab-derived fluids (Wanke et al. 2019) produce magmas with an arc-like geochemical signature. Similar conclusions were drawn for the occurrence of Nb-rich basalts from Borneo (Macpherson et al. 2010). At Mount St Helens, the degree of whole-rock trace element heterogeneity decreases with increasing SiO_2, consistent with mixing and homogenisation of melts during the earliest stages of fractionation (Leeman & Smith 2019; Wanke et al. 2019). From 55 to 70 wt% SiO_2, whole-rock concentrations of trace elements such as Nb, Zr, La, Sm, Y and Yb are approximately constant or decrease slightly whereas La/Yb increases slightly and Sm/Yb is flat (see Figure 6). These trace element patterns are generally not consistent with generation of the more evolved rocks by low-pressure fractional crystallisation from primitive parental magmas, which would result in incompatible behaviour for these elements (Smith and Leeman 1987, 1993; Gardner et al. 1995; Blundy et al. 2008; Pallister et al. 2008; Sisson et al. 2014). Although the erupted magmas contain various cumulate gabbro inclusions (Scarfe and Fujii 1987; Heliker 1995), U-Pb dates for zircons from these samples show that they are not cognate to the Mount St Helens system but derive from an older (Miocene) intrusion (Pallister et al. 2008, 2017). Amphibole equilibrium melts from MgHst-Tsch also show approximately constant (though scattered) HFSE and HREE, concentrations, and slightly increasing La/Yb, constant Sm/Yb and decreasing Dy/Yb from 55-70 wt% SiO_2 (Figure 6). In contrast, the melt inclusions show increasing LREE, MREE and HFSE concentrations and decreasing La/Yb and Sm/Yb but nearly constant Dy/Yb, consistent with low-pressure fractionation of plagioclase and MgHbl (Blundy et al. 2008). This suggests that the conditions for generation of intermediate melts (as sampled by MgHst-

Tsch) were different from the formation conditions of more evolved rhyodacite and rhyolite melts, as sampled by the melt inclusions.

The trace element patterns of whole rocks have previously been ascribed to (i) melting in the presence of garnet, which would retain HFS and HREE (Smith and Leeman 1987), (ii) mixing of replenishing primitive melts with either highly evolved residual liquids or with low degree partial melts of older crustal materials (Pallister et al. 2008; Claiborne et al. 2010; Sisson et al. 2014), and (iii) high pressure fractionation in the presence of garnet, amphibole and/or ilmenite (Blundy et al. 2008). Recent experiments show that the dacite is not in equilibrium with garnet at near-liquidus conditions between 400 and 1200 MPa, indicating that amphibole ± oxide is a better candidate to retain HFS and MREE-HREE in evolved melts at high pressure (Blatter et al. 2017). The REE compositions of our calculated AEMs show increasing La/Yb, constant Sm/Yb and decreasing Dy/Yb with increasing SiO_2 (Figure 6). These patterns are consistent with fractionation of amphibole ± clinopyroxene (Davidson et al. 2007).

The MgHst-Tsch amphiboles themselves are similar to near-liquidus experimental amphiboles produced from Mount St Helens dacite at 700-900 MPa (Blatter et al. 2017). Those experiments also generated liquids similar to the more evolved end of our AEM array, and similar to the least evolved melt inclusions reported by Blundy et al. (2008). Our AEM data therefore support suggestions that while dacite magmas with a trace element signature depleted in HFS and HREE could be formed through intermediate pressure fractionation involving amphibole, they could also be generated through partial (re)-melting of amphibole-bearing gabbros (Blatter et al. 2017).

Our amphibole dataset contains crystals with normal zoning and those with reverse zoning, suggesting that both mixing and fractionation are occurring. This is also consistent with some plagioclase zoning profiles (Smith and Leeman 1987; Streck et al. 2008; Cashman and Blundy 2013) and with co-variations between crystallinity, composition and inferred temperature of whole-rocks (Gardner et al. 1995). We suggest, therefore, that andesite and primitive dacite melts fractionate a mafic assemblage

including amphibole (MgHst-Tsch) ± pyroxene ± Fe-Ti oxide ± plagioclase at moderately high pressures (e.g. >400 MPa; (Alonso-Perez et al. 2009; Blatter et al. 2017). At these mid-crustal pressures, plagioclase crystallisation is suppressed relative to other phases as a result of high water concentrations (Eggler 1972; Blundy and Cashman 2001; Thornber et al. 2008; Melekhova et al. 2015; Blatter et al. 2017), consistent with the relatively shallow decrease of Sr with increasing SiO_2 in the AEM (Figure 4). Mixing between multiple small aliquots of fractionating melt over time, as well as with partial (re-)melts of older intrusive materials also contributes to the formation of a range of dacite magmas. The magmas ascend to shallow pressures (<300 MPa) where crystallisation is dominated by plagioclase ± MgHbl, resulting in low bulk Ds for HFS and REE. Overall, our new dataset gives a picture of a vertically extensive magma plumbing system, involving mid- to lower-crustal pressure fractionation of a mafic assemblage including amphibole ± pyroxene ± Fe-Ti oxides; and low-pressure fractionation dominated by plagioclase ± MgHbl. It is notable that our calculated AEM do not record any melts more primitive than andesite, and this is consistent with observations that mingled basalts and basaltic andesites typically contain an assemblage of olivine + plagioclase + clinopyroxene ± orthopyroxene (Wanke et al. 2019; Pallister et al. 2017); and this may reflect insufficiently high water concentrations to stabilise amphibole in these primitive melts (e.g. Leeman & Smith 2019; Rea et al. 2012; Gardner et al. 1995).

Partial remelting of older intrusives, or source heterogeneity?

The trace element AEM data show significant scatter towards high Nb, Zr, and REE concentrations at intermediate SiO_2 (Figure 5). These equilibrium melt compositions are supported by rare melt inclusions with elevated Nb, Zr, La and La/Yb, which previously appeared to be conspicuous outliers (Blundy et al. 2008), and are also similar to some Castle Creek dacite whole-rocks with elevated trace element concentrations (Figure 5; data from Wanke et al. in press; Wanke et al. 2019). The absolute Nb concentrations are similar to those of enriched, intraplate-like basaltic whole rocks from Mount St Helens (Leeman et al. 1990), but their major element compositions are more evolved, similar to those from neighbouring Mt Adams (Hildreth and Fierstein 1997; Jicha et al. 2009), which show unusually strong geochemical enrichment with increasing SiO_2. These anomalously Nb-rich AEM compositions

were determined from both amphibole cores with non-enriched rims and from amphibole rims on non-enriched cores, and texturally the crystals show no consistent features that might indicate a distinctive origin. This indicates both mechanical incorporation of Nb-enriched amphibole cores into more geochemically typical Mount St Helens melts; and interaction of geochemically typical amphibole crystals with an incompatible-element enriched *melt*. Some of the Castle Creek era dacite whole-rocks approach our trace-element enriched AEM in composition, albeit showing more muted variations (Figure 5). During the Castle Creek period, intrusion and mixing of basalts and basaltic andesites with the resident dacite occurred (Wanke et al. in press; Wanke et al. 2019), accompanying a shift to hotter, more H_2O-poor dacites (Gardner et al. 1995). This suggests that the AEM may be recording melts, generated during mixing, that are only transiently present in the magmatic plumbing system. In general, however, the compositional variability of melts recorded by the AEM exceeds the variability of the andesite-dacite whole rocks, which are relatively homogeneous. We infer that the sub-surface storage and plumbing system can efficiently homogenise diverse melt components that can now only be identified through the distinctive trace element signature that is captured within the compositions of the mineral phases.

Solidification of evolved dacites at within the crust under Mount St. Helens would generate diorites and granodiorites with low-temperature minerals such as biotite, zircon and apatite, as shown by the presence of these as interstitial phases in plutonic inclusions in Mount St Helens magmas (Heliker 1995; Wanke et al. 2019). Although the plutonic inclusions typically have older (Tertiary) zircon ages (Pallister et al. 2017), similar mineralogy is observed in the oldest (Ape Canyon) deposits from Mount St Helens, which included low-temperature dacites and rhyodacites with quartz and biotite (Clynne et al. 2008). Therefore, partial remelting of plutonic residua from earlier intrusive events or magmatic stages would generate disequilibrium melts enriched in Zr and HREE (from zircon), LREE (from apatite) and Ba, Rb and Nb (from biotite) (Villaros et al. 2009; McLeod et al. 2012). The scattered trace element enrichments seen in the AEM could be generated by mixing with limited quantities of such partial melts. This model is consistent with the presence of rare biotite inclusions in amphibole phenocrysts from the 1980s magmas (this study, Loewen 2013) and in older tephras (Smith and

Leeman 1987); with the presence of zircons with significantly older ages in magmas from all eruptive periods, indicating recycling of older components (Claiborne et al. 2010); and with the decoupling of Ra-Th and U-Th ages of plagioclase crystals, which can also be explained by mechanical mixtures of older recycled crystals and younger overgrowths (Cooper and Reid 2003). The higher Zr concentrations of whole rocks than AEM (Figure 5) are also consistent with some mechanical incorporation of zircon into the whole rocks, notwithstanding the scatter and uncertainty on the calculated AEM. This finding emphasises the importance of repeated episodes of intrusion and remobilisation during the formation of arc magmas, and the efficiency of the shallow magma storage system in homogenising diverse inputs. We suggest that the extent of partial melting would be controlled by the local heat flux, available volatile contents and the solid mineral assemblage of the plutonic component, resulting in localised variations in the absolute concentrations of different trace elements.

Finally, it is also possible that the trace elements of amphiboles are reflective of mantle source heterogeneity. The concentrations of Nb in the most enriched AEM are similar to those of the high-Nb basalts erupted at Mount St Helens, derived from an enriched source, even though the major element compositions are more evolved. It is therefore plausible that some amphiboles (perhaps those with 'enriched' cores) actually represent components of differentiating intraplate-like magmas within the plumbing system at Mount St Helens. In principle this hypothesis could be tested using fluid-mobile elements or other indicators of earlier metasomatism; in addition careful petrographic observation of Cascades amphiboles is now required to examine any characteristic textural indications of a distinct origin.

Summary – extending the crystal record to the lower crust

Our trace element regression analysis opens up the potential for using amphibole to interrogate the nature of deep crustal melt evolution in arcs and other hydrous magmas. This gives a new way to

understand the complex nature of subterranean magma systems, and the interactions between multiple batches of magma, and between magmas and solid residues from older intrusive events. Amphibole may come early in the fractionation sequence for mafic magmas (Alonso-Perez et al. 2009; Krawczynski et al. 2012; Melekhova et al. 2015), enabling investigation of earlier stages of magma evolution. Unlike olivine and plagioclase, amphibole contains significant concentrations of a broad range of trace elements, and this may permit quantitative modelling of petrogenetic processes. The method is particularly sensitive to minor proportions of chemically distinct components that are otherwise efficiently homogenised during mid- to low-pressure magma fractionation and ascent. Amphibole is stable across a wide variety of magma compositions, and can specifically trace hydrous magmas found in subduction zone systems. Our method is therefore applicable widely, including in cumulate and plutonic rocks, and will help to construct and refine conceptual models of subvolcanic plumbing systems in arcs.

Acknowledgements

Jing Zhang was supported by a Durham Doctoral Studentship (Durham University), China Scholarship Council (201206170178) and National Natural Science Foundation of China (41702362). Madeleine Humphreys was supported by a Royal Society University Research Fellowship. AJRK and ML were supported by National Science Foundation grants 1425491 and 1028707. GFC was supported by a NERC grant (NE/K010824/1). We thank Mark Allen and Ed Llewellin for helpful comments on an earlier version of the manuscript, and John Pallister and Mike Clynne for additional internal reviews that significantly improved the text. We acknowledge Mike Krawczynski and an anonymous reviewer for helpful reviews. We greatly appreciate helpful discussions with Maren Wanke as well as early access to her whole-rock geochemical dataset. Any use of trade, firm, or product names is for descriptive purposes only and does not imply endorsement by the U.S. Government.

Author contributions

JZ, MCSH and AJRK conceived the project. JZ and GFC performed the multiple regression and ML conducted the major and trace element analysis. MCSH and GFC drafted the text and all authors contributed to discussion of the data and writing of the manuscript.

References

Adam J, Green T (2006) Trace element partitioning between mica- and amphibole-bearing garnet lherzolite and hydrous basanitic melt: 1. Experimental results and the investigation of controls on partitioning behaviour. Contrib Mineral Petrol 152:1–17

Adam J, Green TH (1994) The effects of pressure and temperature on the partitioning of Ti, Sr and REE between amphibole, clinopyroxene and basanitic melts. Chem Geol 117:219–233

Adam J, Green TH, Sie SH (1993) Proton microprobe determined partitioning of Rb, Sr, Ba, Y, Zr, Nb and Ta between experimentally produced amphiboles and silicate melts with variable F content. Chem Geol 109:29–49

Alonso-Perez R, Müntener O, Ulmer P (2009) Igneous garnet and amphibole fractionation in the roots of island arcs: experimental constraints on andesitic liquids. Contrib Mineral Petrol 157:541. doi: DOI 10.1007/s00410-008-0351-8

Bacon CR, Bruggman PE, Christiansen RL, et al (1997) Primitive magmas at five Cascades volcanic fields: melts from hot, heterogeneous sub-arc mantle. Can Mineral 35:397–423

Berlo K, Blundy J, Turner S, Hawkesworth C (2007) Textural and chemical variation in plagioclase phenocrysts from the 1980 eruptions of Mount St. Helens, USA. Contrib Mineral Petrol 154:291–308. doi: 10.1007/s00410-007-0194-8

Blatter DL, Sisson TW, Hankins WB (2017) Voluminous arc dacites as amphibole reaction-boundary liquids. Contrib Mineral Petrol 172:27:27. doi: 10.1007/s00410-017-1340-6

Blundy J, Cashman K (2001) Ascent-driven crystallisation of dacite magmas at Mount St Helens, 1980–1986. Contrib Mineral Petrol 140:631–650. doi: 10.1007/s004100000219

Blundy J, Cashman K (2005) Rapid decompression-driven crystallization recorded by melt inclusions from Mount St. Helens volcano. Geology 33:793–796

Blundy J, Cashman KV, Berlo K (2008) Evolving magma storage conditions beneath Mount St. Helens inferred from chemical variations in melt inclusions from the 1980-1986 and current (2004-2005) eruptions. In: A volcano rekindled: The renewed eruption of

Mount St. Helens, 2004-2006. U.S. Geological Survey Professional Paper 1750, Ed: David R. Sherrod, William E. Scott, and Peter H. Stauffer pp 755–790

Brenan JM, Shaw HF, Ryerson FJ, Phinney DL (1995) Experimental determination of trace-element partitioning between pargasite and a synthetic hydrous andesitic melt. Earth Planet Sci Lett 135:1–11

Cashman K, Blundy J (2013) Petrological cannibalism: the chemical and textural consequences of incremental magma body growth. Contrib Mineral Petrol 166:703–729. doi: 10.1007/s00410-013-0895-0

Cashman KV, McConnell S (2005) Multiple levels of magma storage during the 1980 summer eruptions of Mount St. Helens, WA. Bull Volcanol 68:57–75

Claiborne LL, Miller CF, Flanagan DM, et al (2010) Zircon reveals protracted magma storage and recycling beneath Mount St. Helens. Geology 38:1011–1014

Clynne MA, Calvert AT, Wolfe EW, et al (2008) The Pleistocene eruptive history of Mount St. Helens, Washington, from 300,000 to 12,800 years before present. In: A volcano rekindled: The renewed eruption of Mount St. Helens, 2004-2006. U.S. Geological Survey Professional Paper 1750, Ed: David R. Sherrod, William E. Scott, and Peter H. Stauffer, pp 593-627

Cooper KM, Reid MR (2003) Re-examination of crystal ages in recent Mount St. Helens lavas: implications for magma reservoir processes. Earth Planet Sci Lett 213:149–167

Crummy JM, Savov IP, Navarro-Ochoa C, et al (2014) High-K Mafic Plinian Eruptions of Volcan de Colima, Mexico. J Petrol 55:2155–2192. doi: 10.1093/petrology/egu053

Dalpé C, Baker DR (2000) Experimental investigation of large-ion-lithophile-element-, high-field-strength-element- and rare-earth-element-partitioning between calcic amphibole and basaltic melt: the effects of pressure and oxygen fugacity. Contrib Mineral Petrol 140:233–250

Davidson J, Turner S, Handley H, et al (2007) Amphibole “sponge” in arc crust? Geology 35:787–790

DeBari SM, Greene AR (2011) Vertical stratification of composition, density, and inferred magmatic processes in exposed arc crustal sections. In: Arc-continent collision. Springer-Verlag, Berlin Heidelberg, pp 121–144. Ed: D. Brown and P. Ryan.

Dyar MD, Breves EA, Gunter ME, et al (2016) Use of multivariate analysis for synchrotron micro-XANES analysis of iron valence state in amphiboles. Am Mineral 101:1171–1189

Eggler DH (1972) Amphibole stability in H2O-undersaturated calc-alkaline melts. Earth Planet Sci Lett 15:28–34

Flinders AF, Shen Y (2017) Seismic evidence for a possible deep crustal hot zone beneath Southwest Washington. Sci Rep 7:7400. doi: DOI:10.1038/s41598-017-07123-w

Gardner JE, Carey S, Rutherford MJ, Sigurdsson, Haraldur (1995) Petrologic diversity in Mount St. Helens dacites during the last 4,000 years: implications for magma mixing. Contrib Mineral Petrol 119:224–238

Green TH, Pearson NJ (1985) Experimental determination of REE partition coefficients between amphibole and basaltic to andesitic liquids at high pressure. Geochim Cosmochim Acta 49:1465–1468

Hawthorne FC, Oberti R (2007) Amphiboles: crystal chemistry. Rev Mineral Geochem 67:1–54

Heliker C (1995) Inclusions in Mount St. Helens dacite erupted from 1980 through 1983. J Volcanol Geotherm Res 66:115–135

Hildreth W, Fierstein J (1997) Recent eruptions of Mount Adams, Washington Cascades, USA. Bull Volcanol 58:472–490

Hill GJ, Caldwell TG, Heise W, et al (2009) Distribution of melt beneath Mount St Helens and Mount Adams inferred from magnetotelluric data. Nat Geosci 2:785–789

Hilyard M, Nielsen RL, Beard JS, et al (2000) Experimental determination of the partitioning behaviour of rare earth and high field strength elements between pargasitic amphibole and natural silicate melts. Geochim Cosmochim Acta 64:1103–1120

Holbrook SW, Mooney WD, Christensen NI (1992) The seismic velocity structure of the deep continental crust. In: Continental Lower Crust. Elsevier, Amsterdam, Ed: D.M. Fountain, R. Arculus, and R. Kay pp 1–43.

Izbekov PE, Eichelberger JC, Patino LC, et al (2002) Calcic cores of plagioclase phenocrysts in andesite from Karymsky volcano: Evidence for rapid introduction by basaltic replenishment. Geology 30:799–802

Jicha BR, Hart GL, Johnson CM, et al (2009) Isotopic and trace element constraints on the petrogenesis of lavas from the Mount Adams volcanic field, Washington. Contrib Mineral Petrol 157:189–207

Kiser E, Palomeras I, Levander A, et al (2016) Magma reservoirs from the upper crust to the MOHO inferred from high-resolution Vp and Vs models beneath Mount St. Helens, Washington State, USA. Geology 44:411–414. doi: doi:10.1130/G37591.1

Klein M, Stosch H-G, Seck HA (1997) Partitioning of high field-strength and rare-earth elements between amphibole and quartz-dioritic to tonalitic melts: an experimental study. Chem Geol 138:257–271

Krawczynski MJ, Grove TL, Behrens H (2012) Amphibole stability in primitive arc magmas: effects of temperature, H2O content, and oxygen fugacity. Contrib Mineral Petrol 164:317–339. doi: 10.1007/s00410-012-0740-x

LaTourrette T, Hervig RL, Holloway JR (1995) Trace element partitioning between amphibole, phlogopite, and basanite melt. Earth Planet Sci Lett 135:13–30

Leake BE, Woolley AR, Arps CES, et al (1997) Nomenclature of amphiboles: report of the subcommittee on amphiboles of the International Mineralogical Association, Commission on New Minerals and Mineral Names. Can Mineral 35:219–246

Leeman WP, Lewis JF, Evarts RC, et al (2005) Petrologic constraints on the thermal structure of the Cascades arc. J Volcanol Geotherm Res 140:67–105

Leeman WP, Smith DR (2018) The role of magma mixing, identification of mafic magma inputs, and structure of the underlying magmatic system at Mount St. Helens. Am Mineral Press 1925–1944

Leeman WP, Smith DR, Hildreth W, et al (1990) Compositional diversity of late Cenozoic basalts in a transect across the southern Washington Cascades: Implications for subduction zone magmatism. J Geophys Res 95:19561–19582

Li L, Xiong XL, Liu XC (2017) Nb/Ta fractionation by amphibole in hydrous basaltic systems: Implications for arc magma evolution and continental crust formation. J Petrol 58:3–28

Locock AJ (2014) An Excel spreadsheet to classify chemical analyses of amphiboles following the IMA 2012 recommendations. Comput Geosci 62:1–11

Loewen MW (2013) Volatile mobility of trace metals in volcanic systems. PhD, Oregon State University

Loewen MW, Kent AJR (2012) Sources of elemental fractionation and uncertainty during the analysis of semi-volatile metals in silicate glasses using LA-ICP-MS. J Anal At Spectrom 27:1502. doi: 10.1039/c2ja30075c

Macpherson CG, Chiang KK, Hall R, et al (2010) Plio-Pleistocene intra-plate magmatism from the southern Sulu Arc, Semporna peninsula, Sabah, Borneo: Implications for high-Nb basalt in subduction zones. J Volcanol Geotherm Res 190:25–38

Martel C, Pichavant M, Holtz F, et al (1999) Effects of fO2 and H2O on andesite phase relations between 2 and 4 kbar. J Geophys Res 104:29453–29470

Mason KR, Grant L, Furlow E (1980) The economic effects of the eruptions of Mount St. Helens. U.S. International Trade Commission publication 1096, 84 pp

McLeod CL, Davidson JP, Nowell GM, de Silva SL (2012) Disequilibrium melting during crustal anatexis and implications for modeling open magmatic systems. Geology 40:435–438

Melekhova E, Blundy J, Robertson R, Humphreys MCS (2015) Experimental evidence for polybaric differentiation of primitive arc basalt beneath St. Vincent, Lesser Antilles. J Petrol 56:161–192

Moore G, Carmichael ISE (1998) The hydrous phase equilibria (to 3 kbar) of an andesite and basaltic andesite from western Mexico: constraints on water content and conditions of phenocryst growth. Contrib Mineral Petrol 130:304–319

Müntener O, Ulmer P (2018) Arc crust formation and differentiation constrained by experimental petrology. Am J Sci 318:64–89

Nakamura M, Shimakita S (1998) Dissolution origin and syn-entrapment compositional change of melt inclusion in plagioclase. Earth Planet Sci Lett 161:119–133

Nandedkar RH, Hürlimann N, Ulmer P, Müntener O (2016) Amphibole-melt trace element partitioning of fractionating calc-alkaline magmas in the lower crust: an experimental study. Contrib Mineral Petrol 171:71. doi: 10.1007/s00410-016-1278-0

Nelson ST, Montana A (1992) Sieve-textured plagioclase in volcanic rocks produced by rapid decompression. Am Mineral 77:1242–1249

Nicholls IA, Harris KL (1980) Experimental rare earth element partition coefficients for garnet, clinopyroxene and amphibole coexisting with andesitic and basaltic liquids. Geochim Cosmochim Acta 44:287–308

Nichols ML, Malone SD, Moran SC, et al (2011) Deep long-period earthquakes beneath Washington and Oregon volcanoes. J Volcanol Geotherm Res 200:116–128

Pallister JS, Clynne MA, Wright HM, et al (2017) Field-trip guide to Mount St. Helens, Washington - An overiew of the eruptive history and petrology, tephra deposits, 1980 pyroclastic density current deposits, and the crater. US Geol Surv Sci Investig Rep 2017–5022–D, 65 pp

Pallister JS, Thornber CR, Cashman KV, et al (2008) Petrology of the 2004-2005 Mount St. Helens lava dome - implications for magmatic plumbing and eruption triggering. In: A volcano rekindled: The renewed eruption of Mount St. Helens, 2004-2006. U.S. Geological Survey Professional Paper 1750, Ed: David R. Sherrod, William E. Scott, and Peter H. Stauffer pp 647–702

Pritchard ME, Gregg PM (2016) Geophysical evidence for silicic crustal melt in the continents: Where, what kind, and how much? Elements 12:121–127. doi: 10.2113/gselements.12.2.121

Prouteau G, Scaillet B (2003) Experimental Constraints on the Origin of the 1991 Pinatubo Dacite. J Petrol 44:2203–2241. doi: 10.1093/petrology/egg075

R Core Team (2013) R: A language and environment for statistical computing. R Foundation for Statistical Computing, Vienna, Austria. URL http://www.R-project.org/

Rea J, Wallace PJ, Clynne MA (2012) Pre-eruptive volatile content of mafic magma from the 2.0-1.7 ka Castle Creek eruptive period, Mount St. Helens. p V53C–2853

Ridolfi F, Renzulli A (2012) Calcic amphiboles in calc-alkaline and alkaline magmas: thermobarometric and chemometric empirical equations valid up to 1,130°C and 2.2 GPa. Contrib Mineral Petrol 163:877–895. doi: 10.1007/s00410-011-0704-6

Rowe MC, Kent AJR, Thornber CR (2008) Using amphibole phenocrysts to track vapor transfer during magma crystallization and transport: An example from Mount St. Helens, Washington. J Volcanol Geotherm Res 178:593–607. doi: 10.1016/j.jvolgeores.2008.01.012

Rutherford MJ, Sigurdsson, Haraldur, Carey S, Davis A (1985) The May 18, 1980, eruption of Mount St. Helens 1. Melt composition and experimental phase equilibria. J Geophys Res 90:2929–2947

Scarfe CM, Fujii T (1987) Petrology of crystal clots in the pumice of Mount St Helens' March 19, 1982 eruption; significant role of Fe-Ti oxide crystallization. J Volcanol Geotherm Res 34:1–14

Schumacher JC (1991) Empirical ferric iron corrections: necessity, assumptions, and effects on selected geothermobarometers. Mineral Mag 55:3–18

Shimizu K, Liang Y, Sun C, et al (2017) Parameterized lattice strain models for REE partitioning between amphibole and silicate melt. Am Mineral 102:2254–2267

Sisson TW (1994) Hornblende-melt trace-element partitioning measured by ion microprobe. Chem Geol 117:331–344

Sisson TW, Salters VJM, Larson PB (2014) Petrogenesis of Mount Rainier andesite: Magma flux and geologic controls on the contrasting differentiation styles at stratovolcanoes of the southern Washington Cascades. GSA Bull 126:122–144

Smith DR, Leeman WP (1993) The origin of Mount St. Helens andesites. J Volcanol Geotherm Res 55:271–303

Smith DR, Leeman WP (1987) Petrogenesis of Mount St. Helens dacitic magmas. J Geophys Res 92:10313–10334

Streck MJ (2008) Mineral textures and zoning as evidence for open system processes. Rev Mineral Geochem 69:595–622

Streck MJ, Broderick CA, Thornber CR, et al (2008) Plagioclase populations and zoning in dacite of the 2004-2005 Mount St. Helens eruption: constraints for magma origin and dynamics. In: A volcano U.S. Geological Survey Professional Paper 1750, Ed: David R. Sherrod, William E. Scott, and Peter H. Stauffer dled: The renewed eruption of Mount St. Helens, 2004-2006. pp 791–808

Taylor SR, McLennan SM (1981) The composition and evolution of the continental crust: rare earth element evidence from sedimentary rocks. Philos Trans R Soc Lond A 301:381–399

Thornber CR, Pallister JS, Lowers HA, et al (2008) Chemistry, mineralogy, and petrology of amphibole in Mount St. Helens 2004-2006 dacite. In: A volcano rekindled: The renewed eruption of Mount St. Helens, 2004-2006. U.S. Geological Survey Professional Paper 1750, Ed: David R. Sherrod, William E. Scott, and Peter H. Stauffer pp 727–754

Tiepolo M, Bottazzi P, Foley SF, et al (2001) Fractionation of Nb and Ta from Zr and Hf at mantle depths: the role of titanian pargasite and kaersutite. J Petrol 42:221–232

Tiepolo M, Oberti R, Zanetti A (2007) Trace-element partitioning between amphibole and silicate melt. Rev Mineral Geochem 67:417–452

Tiepolo M, Vannucci R, Bottazzi P, et al (2000a) Partitioning of rare earth elements, Y, Th, U, and Pb between pargasite, kaersutite, and basanite to trachyte melts: Implications for percolated and veined mantle. Geochem Geophys Geosystems 1:n/a–n/a. doi: 10.1029/2000GC000064

Tiepolo M, Vannucci R, Oberti R, et al (2000b) Nb and Ta incorporation and fractionation in titanian pargasite and kaersutite: crystal–chemical constraints and implications for natural systems. Earth Planet Sci Lett 176:185–201. doi: 10.1016/S0012-821X(00)00004-2

Villaros A, Stevens G, Moyen J-F, Buick IS (2009) The trace element compositions of S-type granites: evidence for disequilibrium melting and accessory phase entrainment in the source. Contrib Mineral Petrol 158:543–561

Wanke, M., Karakas, O., & Bachmann, O. (in press) The genesis of arc dacites: the case of Mount St. Helens, WA. Contributions to Mineralogy and Petrology (in press)

Wanke M, Clynne MA, von Wykradt-Huchtenbruck A, et al (2019) Geochemical and petrologic diversity of mafic magmas from Mount St. Helens. Contrib Mineral Petrol in revision:

Witze A (2014) Survey probes volcano's depths. Nature 511:136–137

Zhang J, Humphreys MCS, Cooper GF, et al (2017) Magma mush chemistry at subduction zones, revealed by new melt major element inversion from calcic amphiboles. Am Mineral 102:1353–1367

Figure 1.

Host melt composition, temperature and pressure range of the experimental amphiboles used for regression. Data sources given in Table 1. Melt compositions are shown normalised to 100% anhydrous.

Figure 2.

Comparison of measured partition coefficients *vs* those predicted from the multiple regression models given in Table 2, for La, Nb, Yb and Sr. For equivalent plots for the whole suite of elements see supplementary figure 1. Solid grey line is 1:1 relationship. Dashed lines are ±90% prediction interval. Grey bars give ±1σ and 2σ prediction intervals.

Figure 3.

Variation of major elements in Mount St Helens whole rocks (red triangles, sources reported in Blundy et al. 2008; orange triangles, data and sources reported in Wanke et al. in press and Wanke et al. 2019), melt inclusions (filled circles, from Blundy et al. 2008) and amphibole equilibrium melts (AEM; diamonds). AEM are calculated following Zhang et al. (2017) (see supplementary information). Amphiboles used to calculate the AEM are from the 1980 eruptions (this study) and include MgHbl and MgHst-Tsch. AEM from MgHbl (black) agree well with the least evolved melt inclusions. AEM from MgHst-Tsch (blue) extend the melt inclusion trends back towards the whole rocks.

Figure 4.

Comparison of measured (raw) amphibole trace element concentrations (field with blue dashed outline) with calculated amphibole equilibrium melts. Symbols as for figure 3.

Figure 5.

Trace element variations (ppm) for Mount St Helens whole rocks, melt inclusions and amphibole equilibrium melts (AEM). Data sources and symbols as for figure 3, but yellow diamonds show AEM

for rocks erupted during 2004-2006 (data from Thornber et al. 2008). A subset of AEM show significant variability in concentration at intermediate SiO_2, towards enriched compositions. Representative errors bars indicating accuracy (±1σ confidence intervals) are shown for each element, based on regression statistics (see table 2 and supplementary information). Grey bars indicate equilibrium melts for plagioclase as calculated by Berlo et al. (2007).

Figure 6.

Variation of trace element ratios La/Yb, Sm/Yb and Dy/Yb with SiO_2 for amphibole equilibrium melts, melt inclusions and whole rocks from Mount St. Helens. Symbols as for figure 5.

Figure 7.

Europium anomaly for amphibole equilibrium melts and a subset of whole rocks for which data are available. Symbols as for Figure 5. $Eu/Eu^* = Eu_N/\sqrt{(Sm_N*Gd_N)}$ where subscript N indicates normalisation to chondrite values (Taylor and McLennan 1981).

Table 1.

Run conditions and crystallisation products of published experimental studies used for multiple regression analysis. References cited: Nicholls and Harris 1980; Green and Pearson 1985; Adam et al. 1993; Adam and Green 1994, 2006; Sisson 1994; LaTourrette et al. 1995; Klein et al. 1997; Dalpé and Baker 2000; Hilyard et al. 2000; Tiepolo et al. 2000a; b, 2001, 2007; Nandedkar et al. 2016; Li et al. 2017.

Table 2.

Results of multiple linear regression analysis. Compositional parameters are stoichiometric formula components calculated following the "average ferric" approach of Leake et al. (1997). N, number of measurements used. [a] Prediction intervals for the regression.

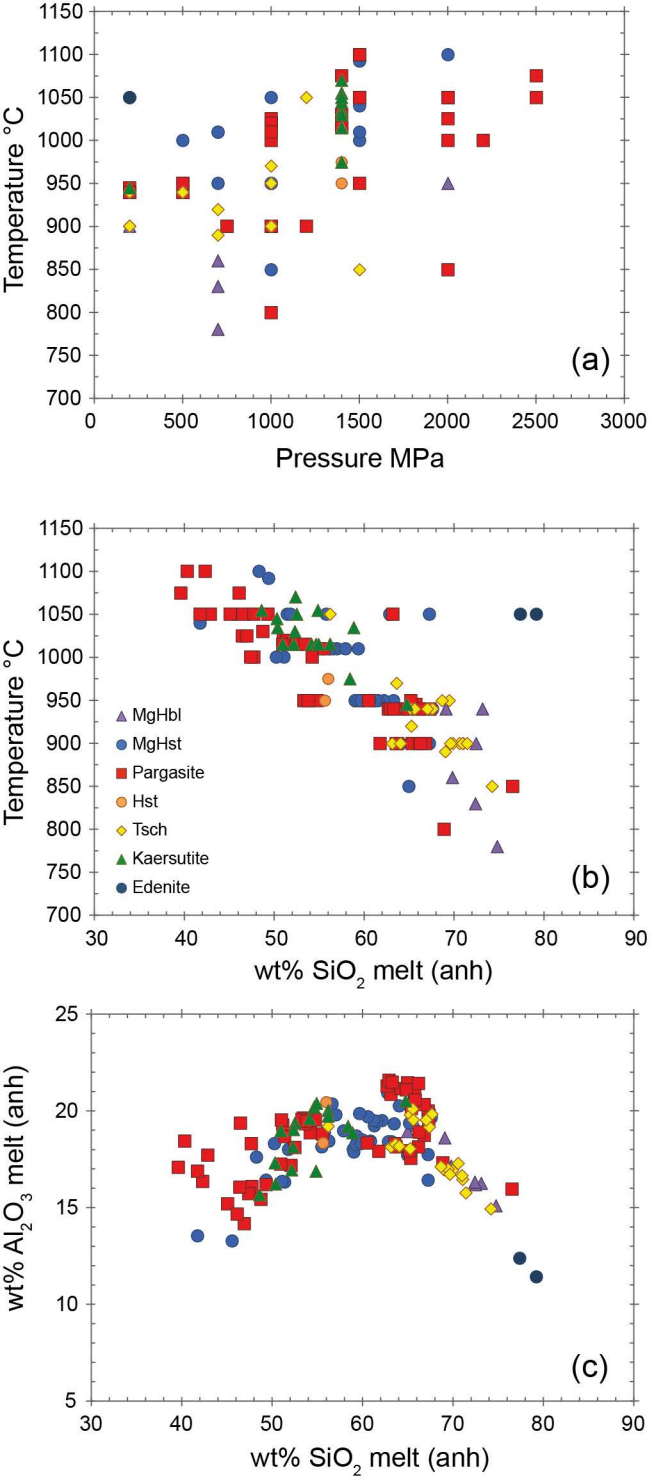
Temperature °C
Pressure MPa
(a)
Temperature °C
wt% SiO2 melt (anh)
MgHbl
MgHst
Pargasite
Hst
Tsch
Kaersutite
Edenite
(b)
wt% Al2O3 melt (anh)
wt% SiO2 melt (anh)
(c)

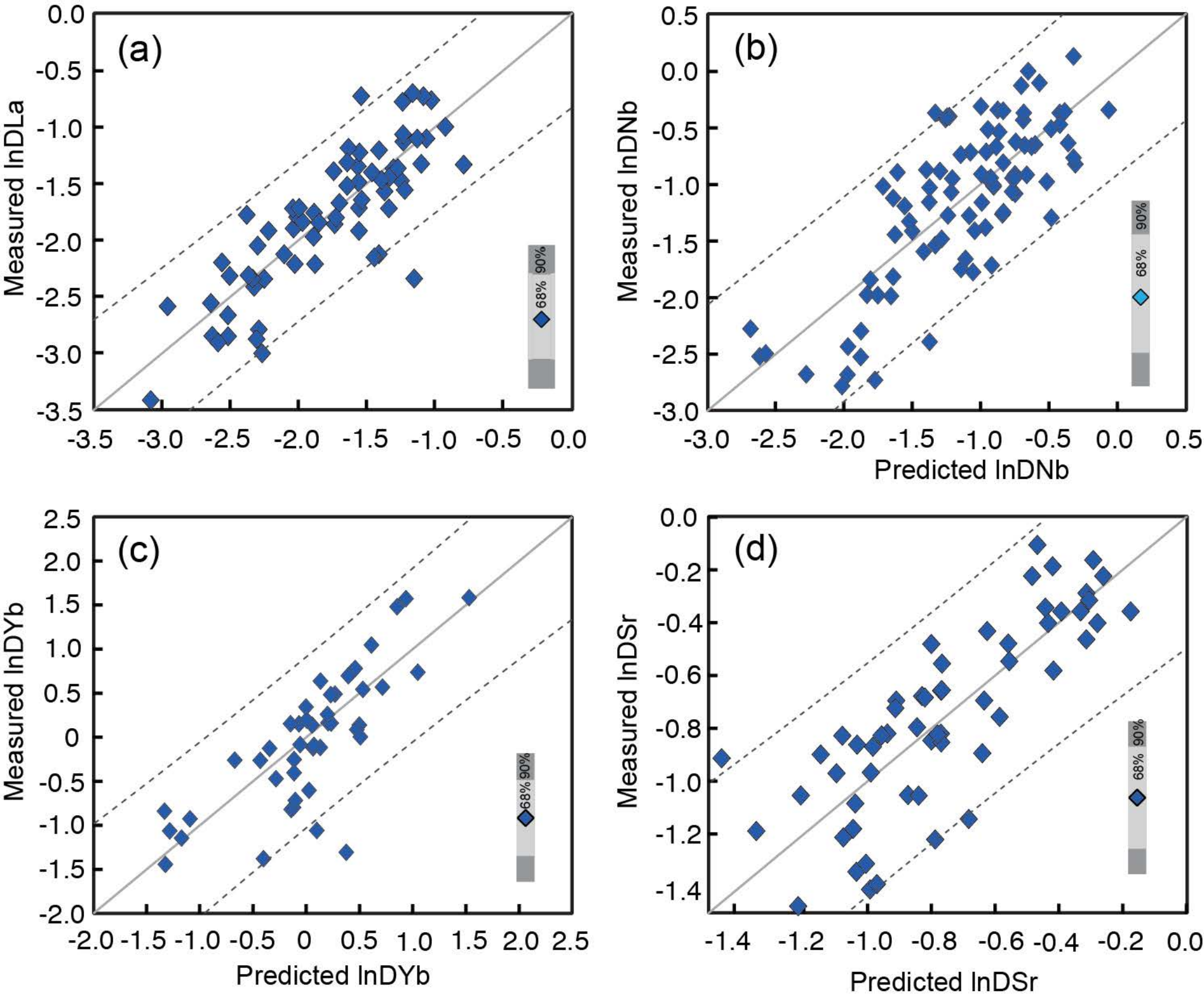
(a)
Measured lnDLa
0.0
-0.5
-1.0
-1.5
-2.0
-2.5
-3.0
-3.5
-3.5 -3.0 -2.5 -2.0 -1.5 -1.0 -0.5 0.0
68% 90%
(b)
Measured lnDNb
0.5
0.0
-0.5
-1.0
-1.5
-2.0
-2.5
-3.0
-3.0 -2.5 -2.0 -1.5 -1.0 -0.5 0.0 0.5
Predicted lnDNb
68% 90%
(c)
Measured lnDYb
2.5
2.0
1.5
1.0
0.5
0
-0.5
-1.0
-1.5
-2.0
-2.0 -1.5 -1.0 -0.5 0 0.5 1.0 1.5 2.0 2.5
Predicted lnDYb
68% 90%
(d)
Measured lnDSr
0.0
-0.2
-0.4
-0.6
-0.8
-1.0
-1.2
-1.4
-1.4 -1.2 -1.0 -0.8 -0.6 -0.4 -0.2 0.0
Predicted lnDSr
68% 90%

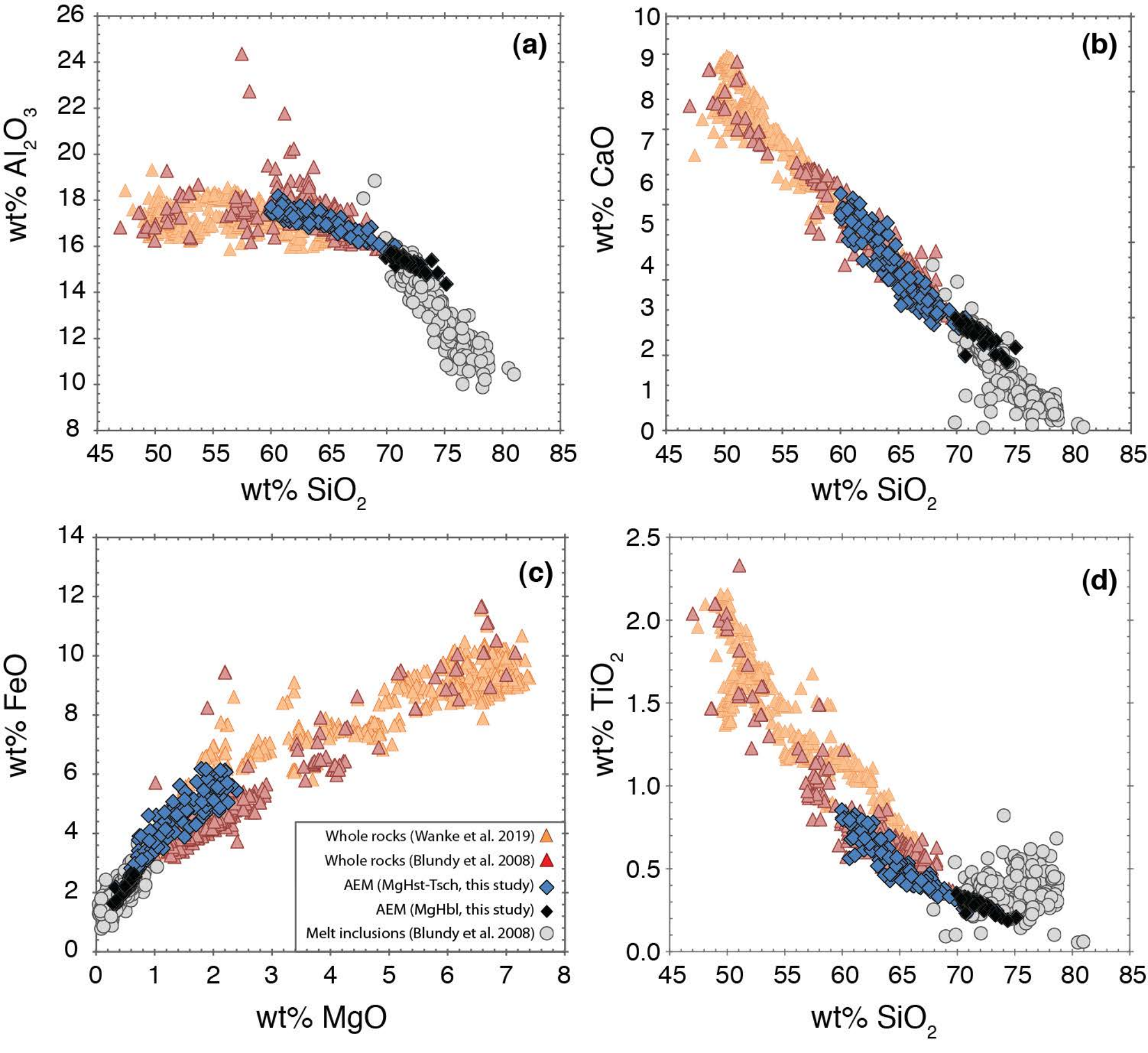
(a)
wt% Al_2O_3
wt% SiO_2
(b)
wt% CaO
wt% SiO_2
(c)
wt% FeO
wt% MgO
(d)
wt% TiO_2
wt% SiO_2
Whole rocks (Wanke et al. 2019)
Whole rocks (Blundy et al. 2008)
AEM (MgHst-Tsch, this study)
AEM (MgHbl, this study)
Melt inclusions (Blundy et al. 2008)

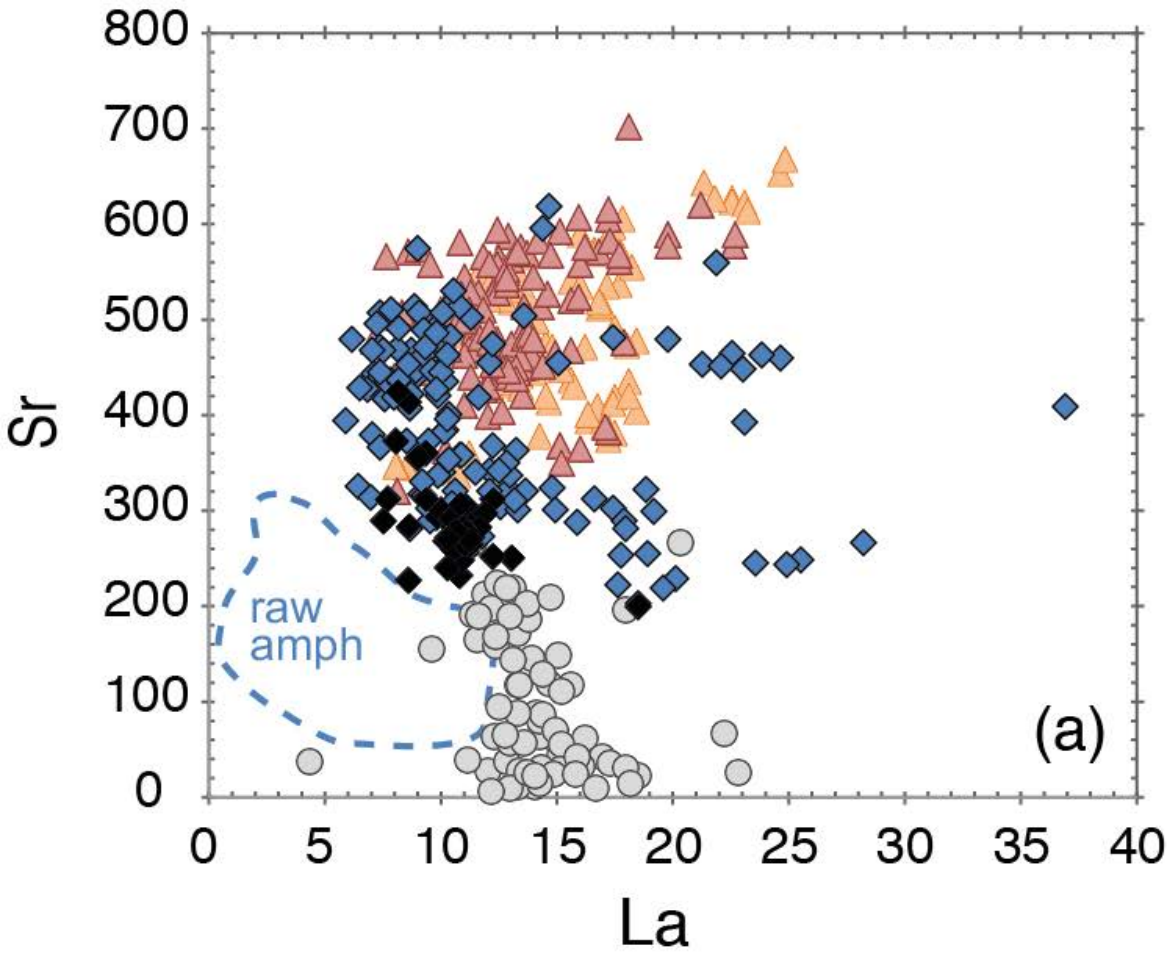
Sr
La
raw
amph
(a)
0
100
200
300
400
500
600
700
800
0
5
10
15
20
25
30
35
40

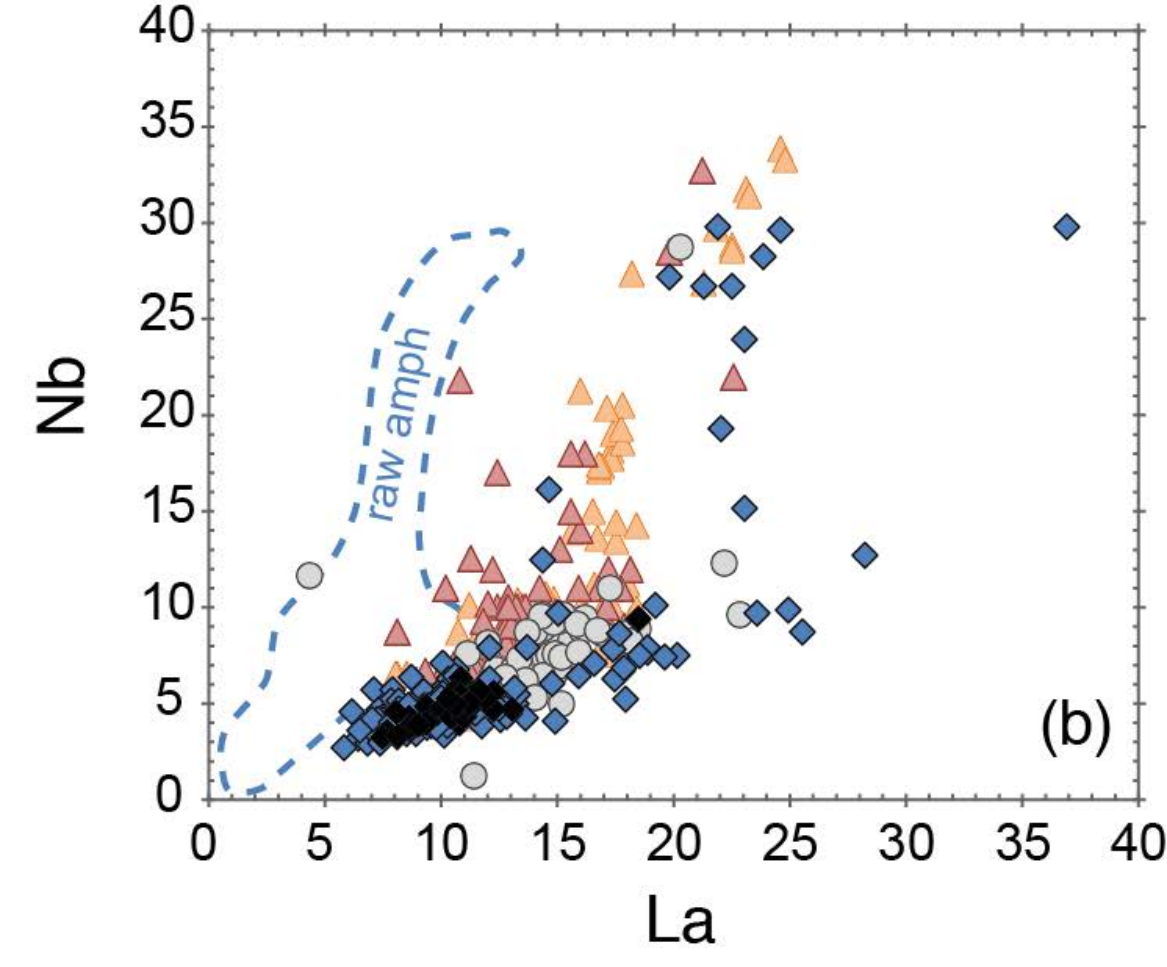
Nb
La
raw amph
(b)
0
5
10
15
20
25
30
35
40
0
5
10
15
20
25
30
35
40

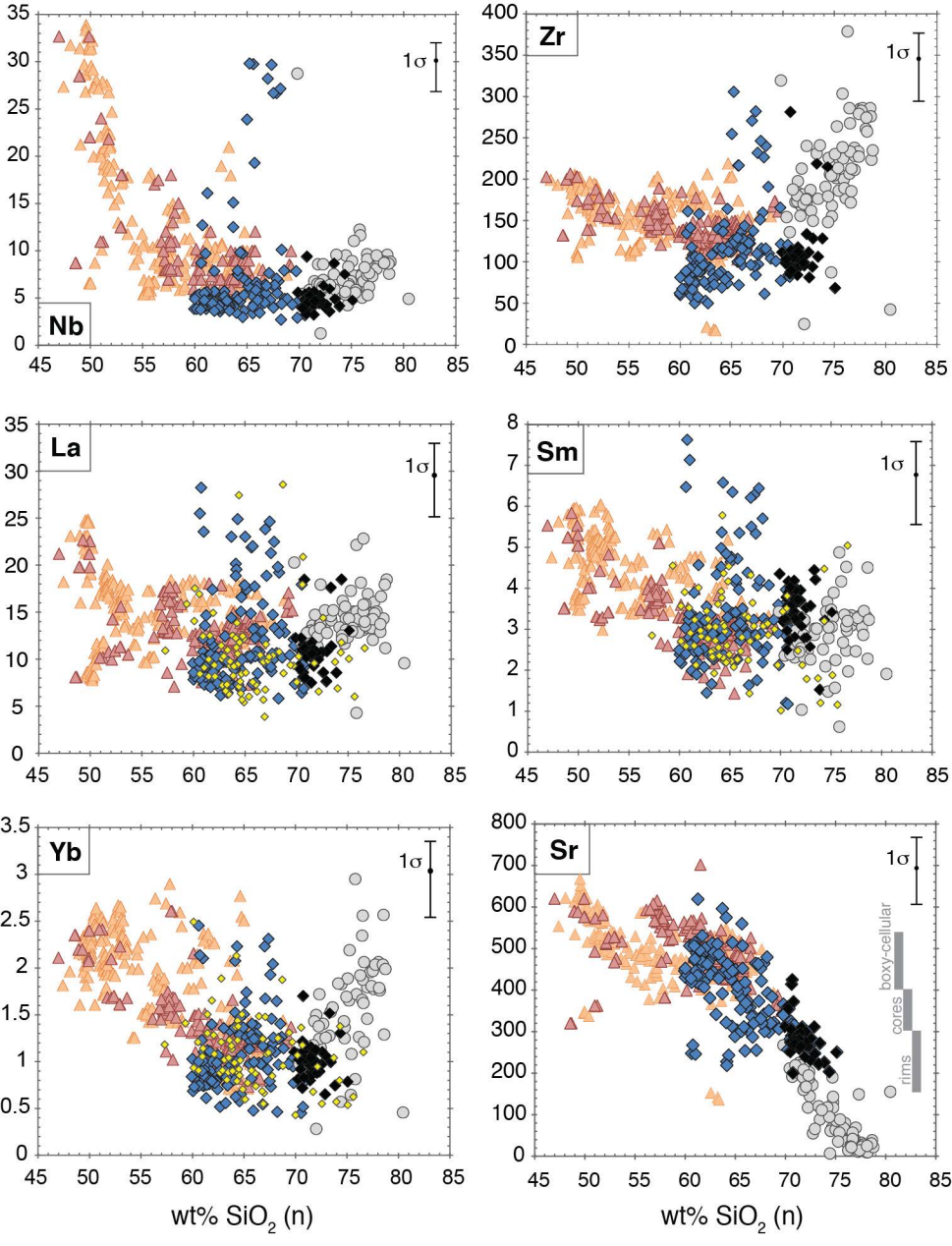
Nb
Zr
La
Sm
Yb
Sr
1σ
boxy-cellular
cores
rims
wt% SiO2 (n)
wt% SiO2 (n)

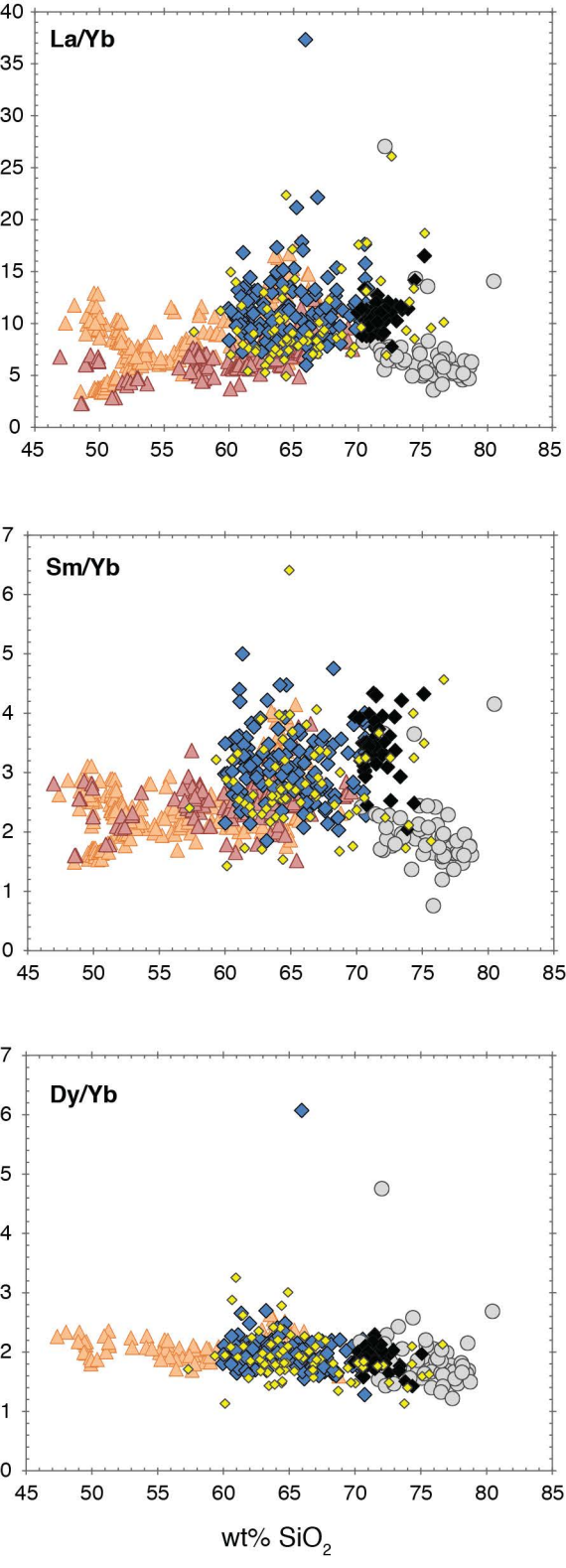
La/Yb
Sm/Yb
Dy/Yb
wt% SiO2

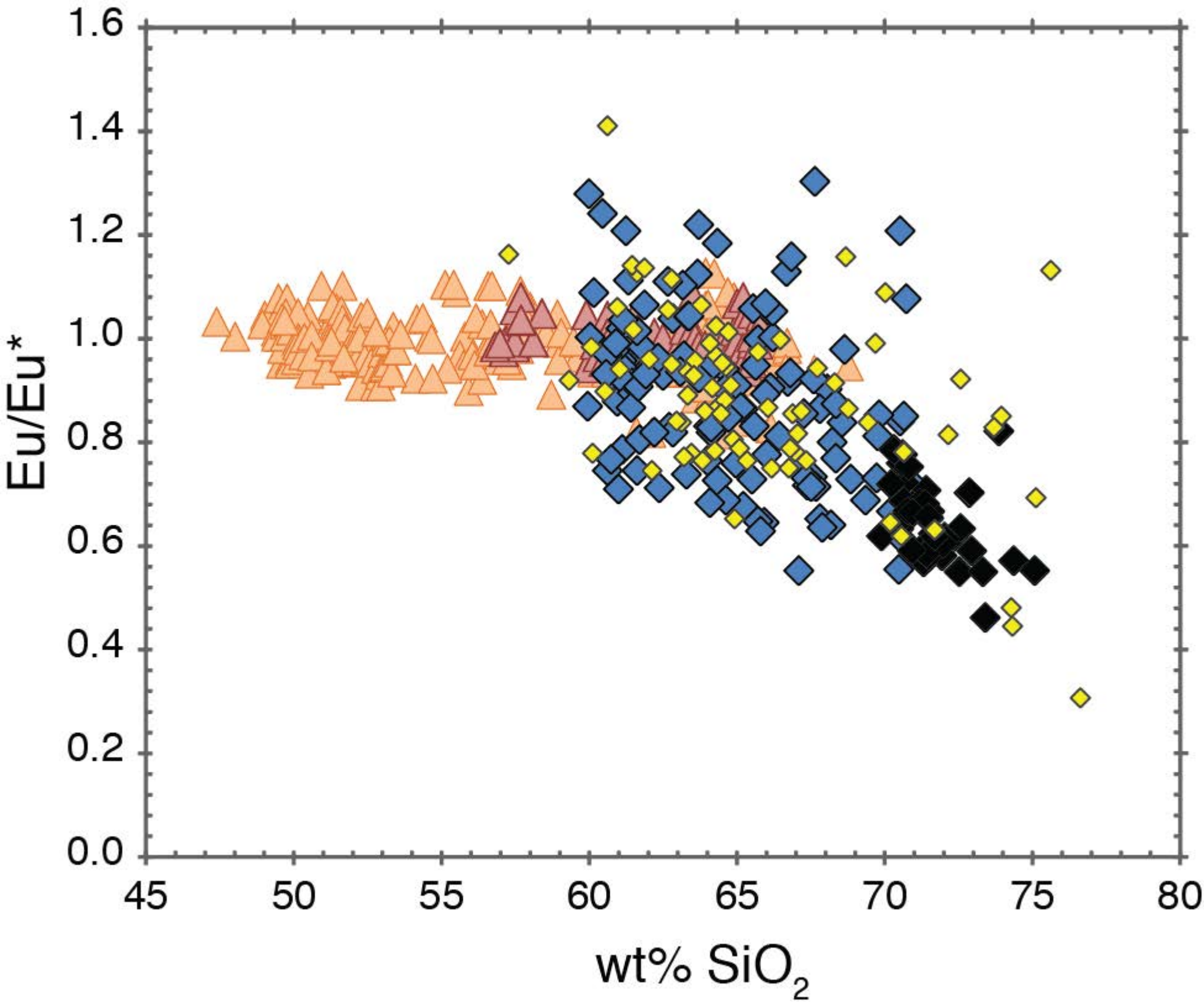
1.6
1.4
1.2
1.0
0.8
0.6
0.4
0.2
0.0
Eu/Eu*
45
50
55
60
65
70
75
80
wt% SiO2

Table 1. Run conditions and crystallisation products of published experimental studies used for multiple regression analysis.

Experimental Study	Starting compositions	n	Pressure (MPa)	Temperature (°C)	Amphibole species
Adam et al. (1993)	basanite-basalt	6	1000-2000	925-1050	MgHbl, MgHst, Parg
Adam & Green (1994)	basanite	6	500-2000	1000-1100	MgHst
Adam & Green (2006)	basanite	2	1000-2000	1025-1050	MgHst
Dalpé & Baker (2000)	basanite-basalt	8	1500-2500	1000-1100	MgHst, Parg
Green & Pearson (1985)	andesite	5	750-2000	900-1050	Tsch, MgHst
Hilyard et al. (2000)	dacite-tonalite	35	200-500	900-945	Tsch, MgHst, MgHbl
Klein et al. (1997)	dacite	3	1000	800-900	Parg, Tsch
LaTourrette et al. (1995)	basanite	1	1500	1150	MgHst
Nicholls & Harris (1980)	basalt-andesite	9	1000	900-1020	Tsch, Parg, MgHst
Nandedkar et al. (2016)	basalt-andesite-rhyolite	8	700	780-1010	MgHst, Tsch, MgHbl
Sisson (1994)*	basalt-andesite-dacite-rhyolite	5	200	1050	MgHst, Edenite
Tiepolo et al. (2000a; 2000b; 2001; 2007)	basalt-andesite	25	1400	1070	MgHst, Kaer, Hastingsite
Li et al. (2017)	basalt	32	500-2000	850-1010	MgHst, Tsch

*This study is a natural material with the matrix rehomogenised at the stated conditions.

Table 2. Results of multiple linear regression analysis. Compositional parameters are stoichiometric formula components calculated following the "average ferric" approach of Leake et al. (1997). n, number of meas

Equation	Dependent variable	D range	Constant	Si	Al^{vi}	Ti	Fe^{3+}	Fe^{2+}	Ca	Na(A)	n	Adjusted R^2	Residual standard error	± 90% §	± 68% §
1	ln DRb	0.05 - 1.04	9.1868	-1.3898		-3.6797	-1.5769	-0.6938			36	0.85	0.29	0.53	0.32
2	ln DSr	0.22 - 0.90	3.41585	-0.75281				0.36529			59	0.64	0.19	0.33	0.20
3	ln DPb	0.03 - 0.17	-4.2533		2.7155	1.69	0.7065			-1.0433	27	0.57	0.23	0.41	0.24
4	ln DZr	0.08 - 1.06	-25.6167	2.6183	2.6867	4.838	2.6591	0.6536	2.5248		60	0.46	0.49	0.80	0.49
5	ln DNb	0.06 - 1.14	-22.27	2.3241		3.7633	2.9786	1.44	1.8719		89	0.60	0.45	0.78	0.47
6	ln DLa	0.03 - 0.59	-20.0493	2.0732		2.5498	1.5317	1.117	2.2771	-1.4576	69	0.69	0.34	0.59	0.36
7	ln DCe	0.08 - 4.23	-21.1078	2.4749		2.4719	1.5722	0.952	1.5311		49	0.82	0.32	0.58	0.34
8	ln DNd	0.18 - 2.46	-20.3082	2.5162		2.5863	1.9459	0.9566	1.2763		45	0.71	0.36	0.64	0.38
9	ln DSm	0.27 - 3.85	-11.3625	1.602			1.2898	1.2376			72	0.60	0.43	0.73	0.44
10	ln DEu	0.28 - 5.8	-35.6604	4.1452	2.6886	6.4057	3.8508	0.7255	3.0679		39	0.77	0.37	0.70	0.42
11	ln DGd	0.33 - 7.22	-19.0583	2.4417		1.9786	1.8765	0.9943	1.3677		54	0.66	0.40	0.71	0.43
12	ln DDy	0.33 - 12.33	-16.0687	2.3858		1.8255	1.9741	0.6922			49	0.79	0.33	0.58	0.35
13	ln DHo	0.32 - 11.66	-20.4148	2.3654		2.484	3.2601	1.2922	3.1762	-4.9224	32	0.90	0.40	0.79	0.47
14	ln DYb	0.24 - 7.83	-15.8659	2.281		1.5905	2.1534	0.7867			48	0.66	0.43	0.45	0.45
15	ln DLu	0.30 - 6.76	-19.3462	2.1142		2.8478	2.7011	1.0402	2.9625	-3.2356	43	0.74	0.39	0.46	0.46
16	ln DY	0.31 - 5.24	-36.2514	3.6078	3.78	7.513	4.8366	0.814	4.6048		61	0.71	0.32	0.37	0.37

§ Prediction intervals for the regression.

Supplementary figure 1.
Comparison of measured partition coefficients with those predicted from regression analysis.

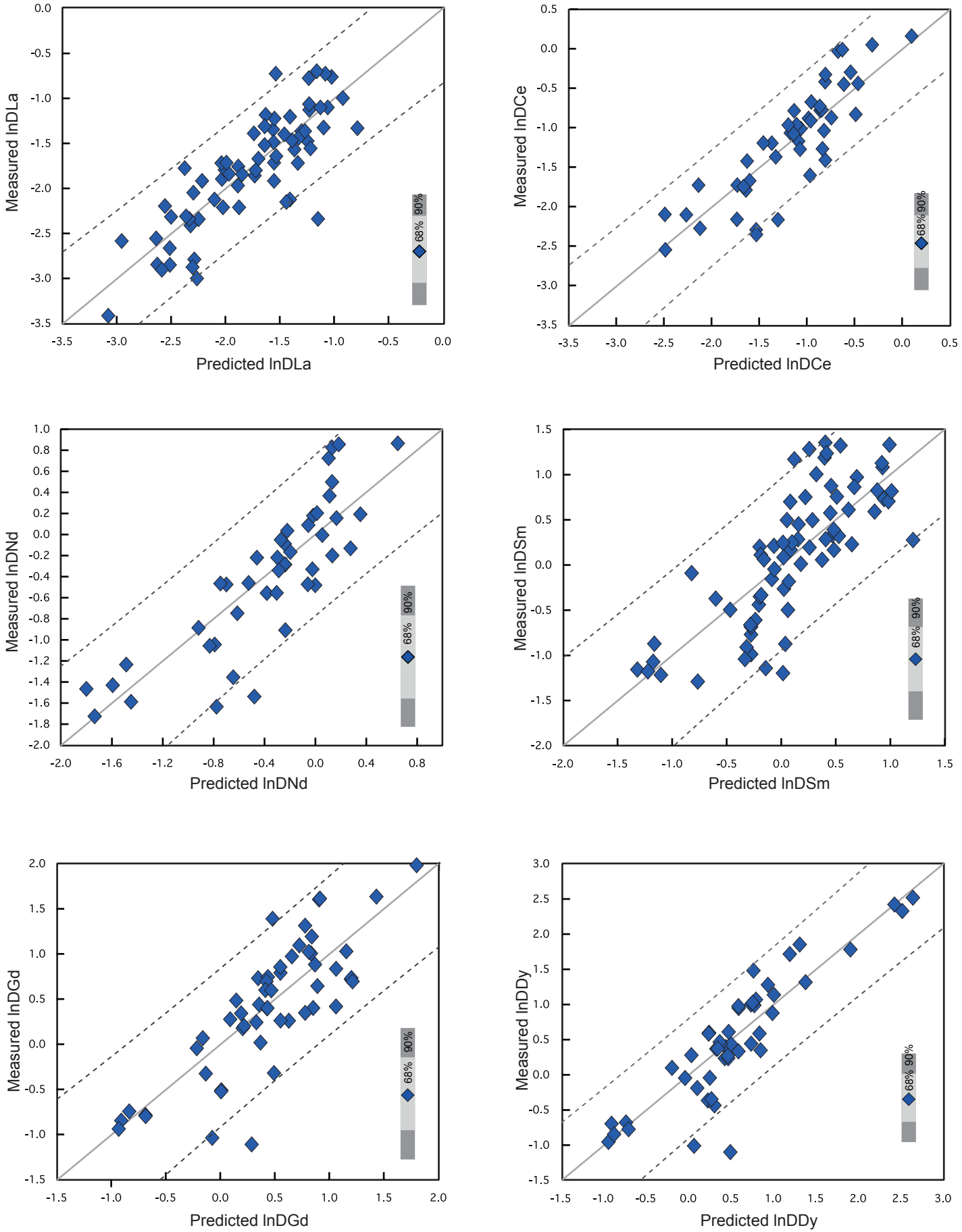

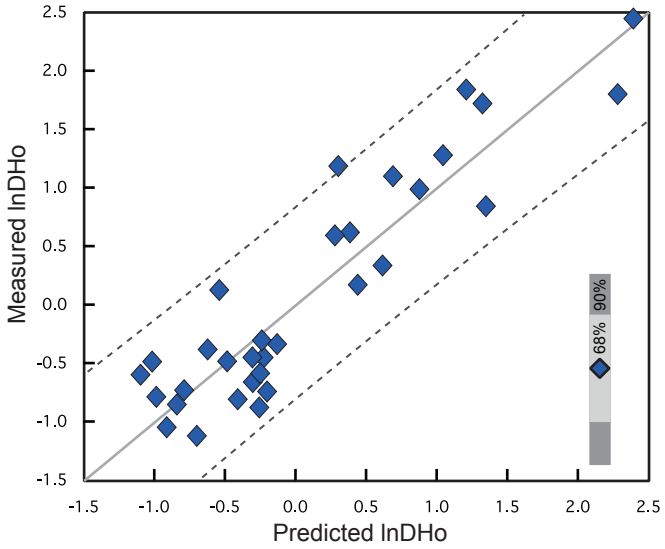
Measured lnDHo
Predicted lnDHo
68%
90%

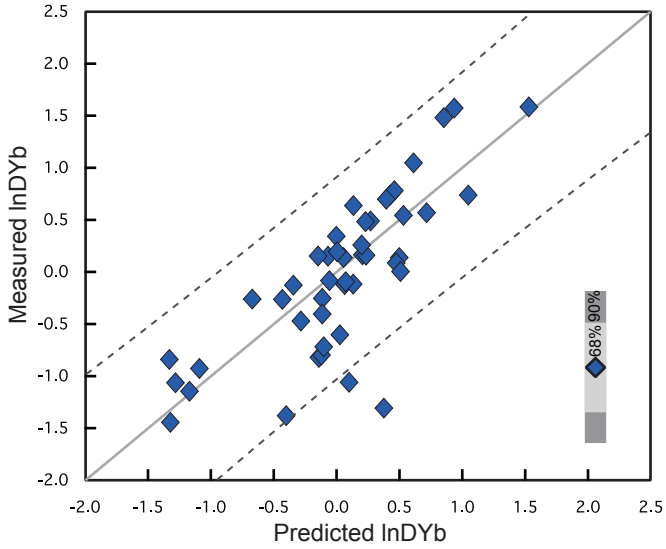
Measured lnDYb
Predicted lnDYb
68%
90%

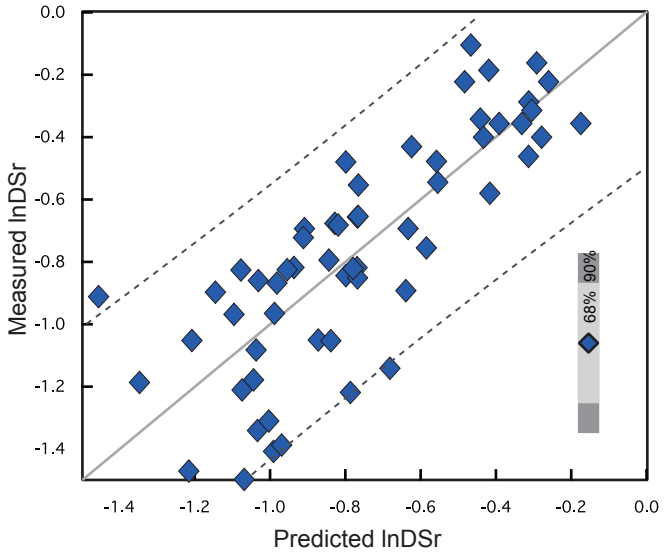
Measured lnDSr
Predicted lnDSr
68%
90%

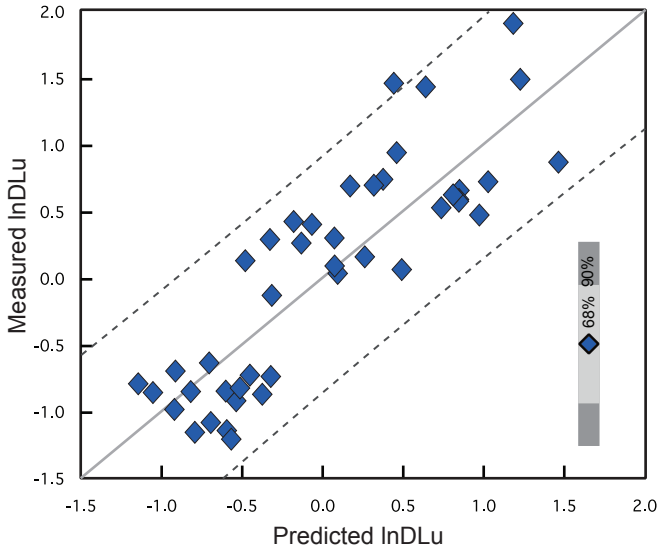
Measured lnDLu
Predicted lnDLu
68%
90%

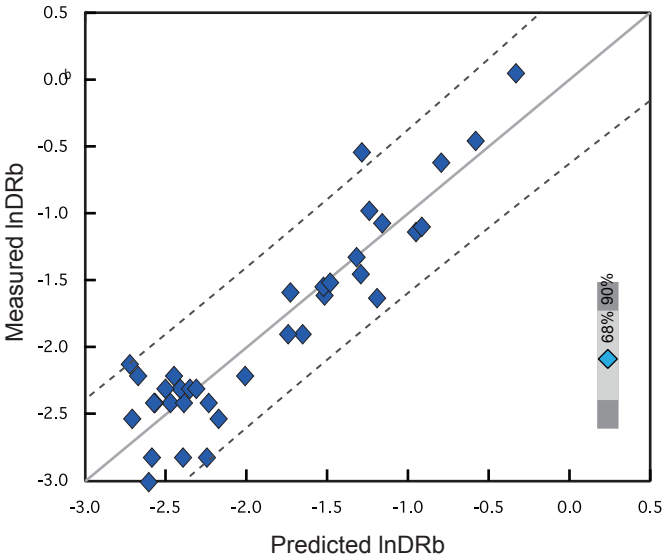
Measured lnDRb
Predicted lnDRb
68%
90%

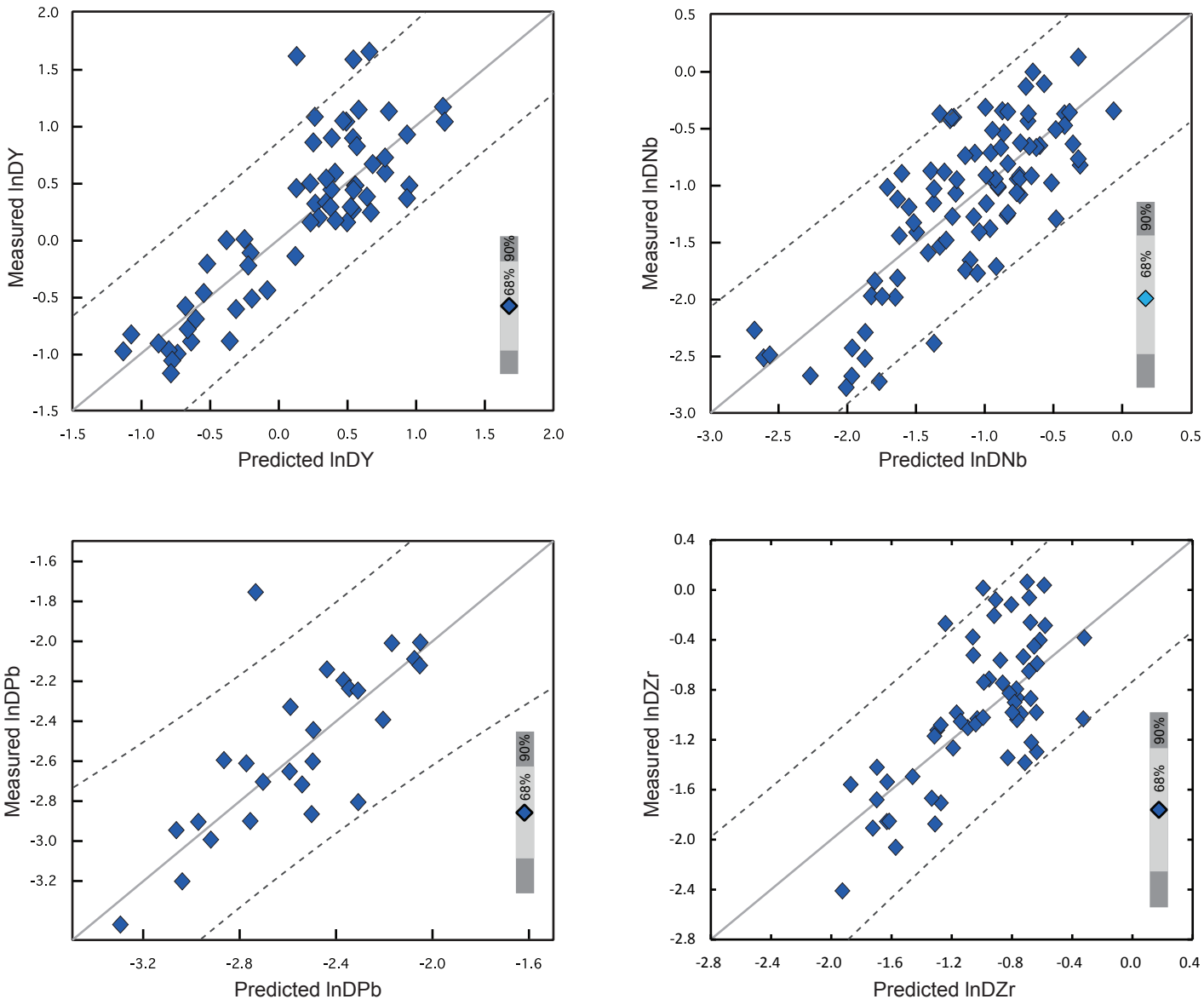
Measured lnDY
Predicted lnDY
68%
90%
Measured lnDNb
Predicted lnDNb
68%
90%
Measured lnDPb
Predicted lnDPb
68%
90%
Measured lnDZr
Predicted lnDZr
68%
90%

Supplementary figure 2.
Comparison of measured partition coefficients with those predicted from regression analysis.
(temperature-dependent regressions)